New Journal of Physics
The open access journal at the forefront of physics

Deutsche Physikalische Gesellschaft DPG IOP Institute of Physics

Quantum Langevin approach for superradiant nanolasers

New Journal of Physics
The open access journal at the forefront of physics

Deutsche Physikalische Gesellschaft DPG
IOP Institute of Physics

Published in partnership with: Deutsche Physikalische Gesellschaft and the Institute of Physics

OPEN ACCESS

RECEIVED
4 December 2020

REVISED
20 April 2021

ACCEPTED FOR PUBLICATION
30 April 2021

PUBLISHED
7 June 2021

PAPER

Quantum Langevin approach for superradiant nanolasers

Igor E Protsenko[1,2,*], Alexander V Uskov[1], Emil C André[2], Jesper Mørk[2,3] and Martijn Wubs[2,3]

[1] Lebedev Physical Institute of RAS, Leninsky prospect 53, Moscow 119991, Russia
[2] Department of Photonics Engineering, Technical University of Denmark, DK-2800 Kgs. Lyngby, Denmark
[3] NanoPhoton—Center for Nanophotonics, Technical University of Denmark, Ørsteds Plads 345A, DK-2800 Kgs. Lyngby, Denmark
[*] Author to whom any correspondence should be addressed.

E-mail: protsen@sci.lebedev.ru

Keywords: laser spectra, superradiance, nanolasers

Abstract

A new approach for analytically solving quantum nonlinear Langevin equations is proposed and applied to calculations of spectra of superradiant lasers where collective effects play an important role. We calculate lasing spectra for arbitrary pump rates and recover well-known results such as the pump dependence of the laser linewidth across the threshold region. We predict new sideband peaks in the spectrum of superradiant lasers with large relaxation oscillations as well as new nonlinear structures in the lasing spectra for weak pump rates. Our approach sheds new light on the importance of population fluctuations in the narrowing of the laser linewidth, in the structure of the lasing spectrum, and in the transition to coherent operation.

1. Introduction

Progress in various technologies has enabled considerable size reductions of lasers. Nowadays quantum dot photonic crystal [1–7], micropillar [8–10], plasmonic [11] and other kinds of nanolasers [12] are intensively investigated. This research is motivated by fundamental questions, such as the minimum size of lasers and the role of quantum effects. The miniaturization of nanolasers is also driven by applications, in nano-electronics for example, where energy-efficient nanolasers are directly incorporated into nano-chips [13–15]. The high density of photon states in nanocavities leads to Purcell enhancement [16] of spontaneous emission into the nanolaser mode, large gain and to the rapid increase of laser power even at small pump rates.

Nowadays there is great interest in *superradiant* lasers, which are lasers that combine a large gain with a small cavity operating in the so-called bad-cavity regime [17–19]. In this regime, the polarization cannot necessarily be adiabatically eliminated and collective spontaneous emission into the lasing mode is significant. Superradiant lasers have been experimentally realized, for example with cold alkaline earth atoms [20–23], rubidium atoms [24], and with quantum dots [25] as the active medium. Superradiant lasers are less sensitive to cavity-length fluctuations, which is important for atomic clocks [20, 21, 24]. Superradiance leads to interesting collective effects, such as excitation trapping [22, 24] and superthermal photon statistics [10, 25, 26], with possible applications in high-visibility optical imaging [27].

An analytical description of superradiant nanolasers and their spectra is complicated by the facts that their quantum noise is not a perturbation, that the equations are nonlinear, and that the polarization of the active medium cannot be adiabatically eliminated. We will address these issues in this paper, where we present an analytical approach to understanding superradiant lasers.

The quantum theory of lasers began with applications of methods of classical statistical radio-physics first for lasers comprising a cavity with high quality (Q) factor [28–30] and later also for low-Q cavity lasers [31, 32]. In many papers the fluctuations of amplitude and phase of laser radiation are considered separately, in the frame of rate equations, where the active-medium polarization is adiabatically eliminated [33–37]. This approach is satisfactory for usual semiconductor lasers and leads to various analytical results,

but the approximations leading to the usual rate equations are not always justified for superradiant nanolasers.

Presently nanolasers are theoretically modeled either by rate equations as in [37, 38], by numerical solution of the density matrix equations as in [22, 39–41], or by systems of equations for correlations as in the cluster expansion [25, 42] or cumulant expansion [43, 44] methods. Numerical analysis of superradiant emission and lasing has recently led to new and interesting results, such as mechanical effects in photon–atom interactions [45], lasing with a millihertz linewidth and rapid emitter number fluctuations [46], Wigner functions for semiconductor heterostructures [47], transition from superradiance to regular lasing by varying the coherent and incoherent driving [44], sub- and superradiance in multimode optical waveguides [48], and photon-antibunching in the fluorescence from an optical nanofiber-tip [49]. However, complementary analytical methods to model nanolasers without adiabatic elimination of polarization, that would apply to superradiant nanolasers, are not well developed.

Here we use Heisenberg–Langevin equations, which are very convenient for the description of lasers [50], to describe systems ranging from LEDs to superradiant nanolasers. The method also describes the limit of non-superradiant lasers, where it will reproduce some well-known results. We follow the approach by Lax, see for example reference [32]: operators are treated as stochastic variables, while quantum properties such as non-vanishing commutation relations are taken into account by diffusion coefficients.

Our first new application of the method will be the description of both the lasing field and the active-medium polarization by symmetric (S) and anti-symmetric (A) combinations of quadrature operators. Quadratures of the polarization have been used in Lamb's semiclassical laser theory [30], while quadratures of the electromagnetic field were used, for example, in the analysis of the driven Van der Pol oscillator applied to lasers in [36] and in quantum optics to squeezed states of the radiation field [50]. Symmetric and anti-symmetric combinations of the quadratures of a quantum field are also used in entanglement criteria [51, 52]. Our work is an extension since, to our knowledge, quadratures as well as their S/A combinations for both the lasing field and polarization combined have not been used in laser theory before. The approach has several advantages: it does not require a quantum phase operator [53], and furthermore we find the equations for the S/A quadrature combinations less cumbersome than for the density matrix [50].

Our second new application is the linearization of the quantum Langevin equations, where fluctuations are not necessarily small compared to mean values. This goes beyond a small-signal analysis (SSA) as, for example, in references [36, 54, 55] and requires other approximations. We describe our method in detail, and it may be useful also for other physical systems with resonant nonlinear interactions of light with matter, see examples in reference [56].

Section 2 introduces the quantum Maxwell–Bloch equations (MBE) with dissipation for a two-level laser and we rederive some key results of semiclassical laser theory [50, 57] to be used for comparison later in the paper.

In section 3 we demonstrate a method, used before in [58, 59], for approximately solving the nonlinear quantum MBE by use of a Fourier transform. With this method, we extend the semiclassical approach by taking into account spontaneous emission into the lasing mode below the semiclassical threshold, where population fluctuations can be neglected. In subsequent sections we do take population fluctuations into account. We obtain the expression for the laser linewidth as a function of the population inversion, as in [59], reproduce the well-known laser linewidth at small excitation, as in [57] and derive the beta-factor for bad-cavity lasers, as in [38], three results to illustrate the efficiency of our method.

Sections 4–6 are the main parts of the paper. In section 4 we represent the lasing field and polarisation by the S- and A-combinations of quadrature-operators, and derive the central linear equations of our approach. We will show that in linear approximation only the S-combinations interact with population fluctuations, while the A-combinations do not. We justify the approximations made to linearize the initial nonlinear MBE.

In section 5 we solve the equations for the A-combinations, show that they describe the laser output power and the linewidth in the high-pump limit, and reproduce the formula for the laser linewidth in that limit.

In section 6 we derive expressions for lasing spectra and show examples of the analysis of spectra for superradiant and non-superradiant lasers. The final two sections contain discussions and our conclusions.

The novelty of our method is that we analytically describe the laser below, near and above the threshold by the same set of stochastic equations, taking into account the field, polarisation and population quantum fluctuations, spontaneous emission into the lasing mode and full laser dynamics without adiabatic elimination of polarization. Such accurate treatment is in particular important for superradiant lasers, where collective effects among the emitters need to be taken into account. With our method we reproduce well-known results and identify features, in particular in the laser spectra, that largely went unnoticed. In

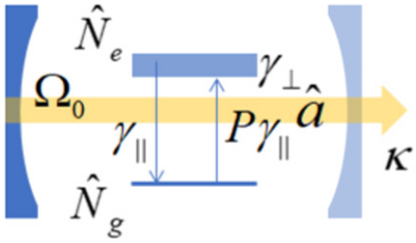

Figure 1. Scheme of the two-level laser, with parameters and operators as defined in the main text. It is common to assume that $\gamma_\perp \gg 2\kappa, \gamma_\parallel$ so that the polarization can be adiabatically eliminated and the laser is well described by rate equations. This does not work for the superradiant nanolasers considered here, where $\gamma_\perp < 2\kappa$.

particular, we calculate the full spectrum of the lasing field below as well as above threshold and identify and explain the appearance of a broad spectral background above threshold and a multi-peak structure above and below threshold. In particular, we focus on the role of population fluctuations and nonlinear polarisation dynamics in superradiant lasers.

2. Quantum Maxwell–Bloch equations. Semiclassical laser model

In order to keep the analysis simple, we consider a stationary single-mode laser, shown schematically in figure 1, with a large number $N_0 \gg 1$ of homogeneously broadened identical two-level emitters, with their transition frequency ω_0 equal to the cavity mode frequency. We write the quantum MBE for such a laser [50] in the rotating-wave approximation with carrier frequency ω_0,

$$\dot{\hat{a}} = -\kappa\hat{a} + \Omega_0\hat{v} + \hat{F}_a \tag{1a}$$

$$\dot{\hat{v}} = -(\gamma_\perp/2)\hat{v} + \Omega_0 f\hat{a}\hat{N} + \hat{F}_v \tag{1b}$$

$$\dot{\hat{N}}_e = -\Omega_0(\hat{a}^+\hat{v} + \hat{v}^+\hat{a}) + \gamma_\parallel(P\hat{N}_g - \hat{N}_e) + \hat{F}_{N_e}. \tag{1c}$$

Here $\hat{a}$ is the annihilation operator of the laser cavity mode, the operator $\hat{v} = i\sum_{i=1}^{N_0} f_i\hat{\sigma}_i$ describes the polarization of the emitters, $\hat{\sigma}_i$ describes transitions from the excited to the ground state of the ith emitter; f_i characterizes the coupling of the ith emitter to the lasing mode. We also define the average square coupling $f = N_0^{-1}\sum_i f_i^2$. Furthermore, Ω_0 is the vacuum Rabi frequency and the total excited- and ground-state population operators $\hat{N}_{e,g}$ are defined as the sums $\sum_{i=1}^{N_0}\hat{n}_i^{(e,g)}$, where $\hat{n}_i^e$ ($\hat{n}_i^g$) are operators of populations of excited (ground) states of the ith emitter. The operator $\hat{N} = \hat{N}_e - \hat{N}_g$ is then the population inversion. In general we use 'hats' to denote operators, while mean values of operators are indicated by the absence of a hat, for example $\langle\hat{N}\rangle = N$. We will consider the stationary case, so mean values do not depend on time. The laser field leaves the cavity through the mirror at the cavity decay rate 2κ; $\gamma_\parallel$ is the population relaxation rate of the upper lasing level, $\gamma_\parallel P$ is the pump rate from the lower to the upper level; $\gamma_\perp/2$ is the polarization relaxation rate (so that $\gamma_\perp$ is the width of the lasing transition). The total number of emitters is assumed preserved, $\hat{N}_e + \hat{N}_g = N_0$, so we can rewrite $\hat{N}_g = N_0 - \hat{N}_e$ and $\hat{N} = 2\hat{N}_e - N_0$.

The quantum operators in equation (1) are interpreted as stochastic variables, where Langevin forces and their associated correlation strengths ensure correct quantum properties. In more detail, we introduced the Langevin forces $\hat{F}_\alpha$, with α taken from the set $\{a, v, a^+, v^+, N_e\}$. These describe white noise, have zero mean (i.e. $\langle\hat{F}_\alpha\rangle = 0$), and are delta-correlated in time: $\langle\hat{F}_\alpha(t)\hat{F}_\beta(t')\rangle = D_{\alpha\beta}\delta(t-t')$, where $D_{\alpha\beta}$ are the diffusion constants. In the Fourier-domain the cross-correlation of these Langevin forces is given by

$$\left\langle\hat{F}_\alpha(\omega)\hat{F}_\beta(\omega')\right\rangle = 2D_{\alpha\beta}\delta(\omega+\omega'). \tag{2}$$

From equation (1a) and its Hermitian conjugate we then obtain

$$0 = -2\kappa n + \Omega_0(\langle\hat{a}^+\hat{v}\rangle + \langle\hat{v}^+\hat{a}\rangle), \tag{3}$$

in terms of the stationary mean photon number $n = \langle\hat{a}^+\hat{a}\rangle$. In combination with equation (1c) we can eliminate the atom-field correlations and obtain the energy conservation law

$$2\kappa n + \gamma_\parallel N_e = \gamma_\parallel P N_g. \tag{4}$$

Stationary solutions of equation (1) are readily obtained, if we neglect the Langevin forces and replace operators by c-numbers: $\hat{a} \to a$, $\hat{v} \to v$, $\hat{N} \to N$. This gives the conventional stationary equations for the

stationary solutions of the semiclassical laser model [50]

$$0 = -\kappa a + \Omega_0 v \tag{5a}$$

$$0 = -(\gamma_\perp/2)v + \Omega_0 f a N \tag{5b}$$

$$0 = -\Omega_0(a^* v + v^* a) + \gamma_\parallel(PN_g - N_e). \tag{5c}$$

Equations (5a) and (5b) have non-vanishing solutions if

$$N > N_{\rm th} \equiv \kappa\gamma_\perp/(2\Omega_0^2 f). \tag{6}$$

From the energy conservation law (4), we find the stationary number of photons in the semiclassical model to be

$$n = \frac{\gamma_\parallel}{2\kappa}(N_0 + N_{\rm th})(P/P_{\rm th} - 1). \tag{7}$$

So the semiclassical model predicts lasing, $n > 0$, when $N_0 > N_{\rm th}$ and when the dimensionless pump rate P exceeds the semiclassical lasing threshold $P_{\rm th}$

$$P > P_{\rm th} = (N_0 + N_{\rm th})/(N_0 - N_{\rm th}). \tag{8}$$

For a dimensionless pump rate P smaller than $P_{\rm th}$, lasing is absent and $n = 0$ in the semiclassical laser model.

3. Analysis neglecting population fluctuations

Nanolasers have large beta factors [60], so that spontaneous emission into the lasing mode is non-negligible [2–5]. Below and close to the semiclassical threshold, nanolasers are not well described by the standard semiclassical model, which neglects spontaneous emission and predicts zero photons. One can improve upon this when $\gamma_\perp \gg 2\kappa, \gamma_\parallel$, in which case polarization can be adiabatically eliminated. This is typically the case for semiconductor lasers. In this case, the laser can be described, for all pump rates, by quantum rate equations (QRE) [38, 60, 61], that do take into account spontaneous emission into the lasing mode. The intensity noise spectra can then also be found by SSA of the QRE [38].

In appendix A we show, following [62], that the condition $2\kappa/\gamma_\perp \geqslant 1$ in our model corresponds to high inter-emitter correlations. So we take this inequality to be a requirement for the low-Q cavities of superradiant lasers [17–19]. In appendix A we also show that lasing with our parameters is possible when the beta-factor is of the order of 1. So here we will refer to nanolasers with $2\kappa/\gamma_\perp \geqslant 1$ and $\beta \geqslant 1$ as superradiant (SR) nanolasers. SR lasing may also be possible when $2\kappa/\gamma_\perp$ and β are smaller than unity, provided that inter-emitter correlations are still large. Here we use $2\kappa/\gamma_\perp \geqslant 1$ and $\beta \geqslant 1$ as sufficient conditions for superradiant lasing.

Since the QRE cannot be applied to superradiant lasers with $\gamma_\perp \leqslant 2\kappa$ and the active-medium polarization cannot be adiabatically eliminated, we must go beyond the QRE. In this section we do this in the low-pump limit. We include the dynamics of the polarization, rather than to eliminate it adiabatically.

Following [58, 59], our main approximation will be that we neglect population fluctuations. This is a good approximation for small pump rates, when the material gain is much smaller than the cavity loss, such that fluctuations of the populations, and thereby of the material gain, do not significantly change the net cavity gain [34]. We also take into account spontaneous emission into the lasing mode and introduce a Fourier-expansion method that is used throughout the paper. We will reproduce the well-known formula for the lasing linewidth in the low-pump limit and introduce the β-factor for lasers with low-quality cavities. These results will be used as a reference for comparison in the following sections, where we do take population fluctuations into account.

Neglecting population fluctuations, we replace population operators in equation (1b) by their mean values

$$\hat{N}_{e,g} \approx N_{e,g}, \qquad \hat{N} \approx N. \tag{9}$$

Thereby equations (1a) and (1b) turn into a set of linear equations

$$\dot{\hat{a}} = -\kappa\hat{a} + \Omega_0\hat{v} + \hat{F}_a \tag{10a}$$

$$\dot{\hat{v}} = -(\gamma_\perp/2)\hat{v} + \Omega_0 f\hat{a}N + \hat{F}_v. \tag{10b}$$

We express $\hat{a}(t)$ and $\hat{v}(t)$ and their corresponding Langevin forces through Fourier-component operators

$$\hat{\alpha}(t) = \frac{1}{\sqrt{2\pi}}\int_{-\infty}^{\infty}\hat{\alpha}(\omega)\mathrm{e}^{-\mathrm{i}\omega t}\,\mathrm{d}\omega \tag{11}$$

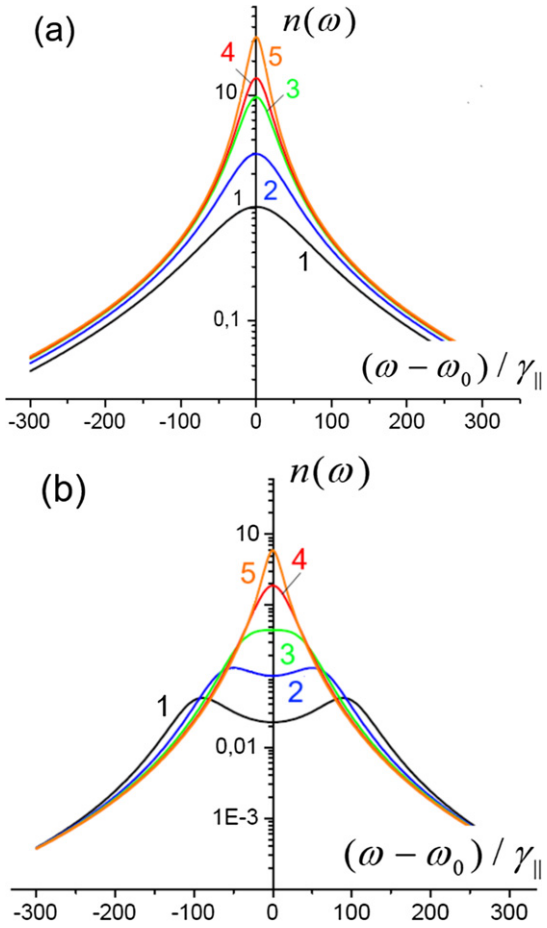

Figure 2. Optical spectrum $n(\omega)$, obtained by neglecting population fluctuations, as given by equation (16). Parameter values: $2\kappa = 100\gamma_{\|}$, $\Omega_0 = 34\gamma_{\|}$, $N_0 = 100$. The scaled pump rates are $P = 2$, 4, 8, 10, and 16 for the curves labeled 1 through 5, respectively. Panel (a): $\gamma_{\perp} = 700\gamma_{\|}$, $N_c = 108 > N_0$. The optical spectrum has only one peak. Panel (b): $\gamma_{\perp} = 50\gamma_{\|}$, $N_c = 2.7 < N_0$. The optical spectrum has two peaks only for the curves 1 and 2, since only for these two are the pump rates P below $P_c = 7.4$.

for $\hat{\alpha} = \{\hat{a}, \hat{v}, \hat{F}_a, \hat{F}_v\}$, and obtain from equation (10) linear algebraic equations for all $\alpha(\omega)$ and find from them

$$\hat{a}(\omega) = \frac{\left(\gamma_{\perp}/2 - i\omega\right)\hat{F}_a(\omega) + \Omega_0\hat{F}_v(\omega)}{(i\omega - \kappa)\left(i\omega - \gamma_{\perp}/2\right) - \Omega_0^2 fN}. \tag{12}$$

Coming back from $\hat{a}(\omega)$ to $\hat{a}(t)$ by an inverse Fourier-transformation, we calculate the mean number of photons in the cavity as

$$n = \langle \hat{a}^{+}(t)\hat{a}(t)\rangle = \frac{1}{2\pi}\int_{-\infty}^{\infty} n(\omega)\mathrm{d}\omega, \tag{13}$$

where $n(\omega)$ is the spectral power density of the field in the lasing mode, or optical spectrum, which is related to $\hat{a}(\omega)$ as

$$\langle \hat{a}^{+}(\omega)\hat{a}(\omega')\rangle = n(\omega)\delta(\omega + \omega'). \tag{14}$$

As a technical aside, in this paper we use Fourier-expansions in terms of $\exp(-i\omega t)$ for all operators, both for $\hat{\alpha}^{+}$ and for $\hat{\alpha}^{+}$ for example. This is why we end up with the factor $\delta(\omega + \omega')$ in equation (14) and in all similar frequency-dependent correlations.

We will determine $n(\omega)$ and then find n by equation (13). In order to find $n(\omega)$ we must know the relevant diffusion coefficients [54, 63]. After neglecting, as is usual, any thermal radiation in the lasing mode, since $k_{\mathrm{B}}T \ll \hbar\omega$, we take the diffusion coefficient $2D_{a^{+}a} = 0$. When population fluctuations are neglected, the diffusion coefficient $D_{v^{+}v}$ becomes

$$2D_{v^{+}v} = f\gamma_{\perp}N_e, \tag{15}$$

as shown in appendix B. With these diffusion coefficients, we find the optical spectrum

$$n(\omega) = \frac{(\kappa\gamma_\perp^2/2)N_e/N_{\rm th}}{[(1-N/N_{\rm th})(\kappa\gamma_\perp/2)-\omega^2]^2+\omega^2(\kappa+\gamma_\perp/2)^2}. \tag{16}$$

This spectrum may either have one or two peaks. Two peaks occur when all emitters are collectively and strongly coupled to the lasing mode, under the condition

$$N_c \equiv \frac{1}{2}\left(\frac{2\kappa}{\gamma_\perp}+\frac{\gamma_\perp}{2\kappa}\right)N_{\rm th} < N_0, \tag{17}$$

and when $P < P_c$, where P_c is such that $N(P_c) = -N_c$. The two peaks in $n(\omega)$ are then caused by and a signature of collective Rabi splitting (CRS) [59]. Otherwise, $n(\omega)$ has a single peak, with full width at half maximum $\gamma_{\rm las}$, defined by $n(\gamma_{\rm las}/2) = n(\omega = 0)/2$, with the value

$$\gamma_{\rm las} = \frac{2\kappa+\gamma_\perp}{\sqrt{2}}\left\{r-1+\sqrt{(r-1)^2+r^2}\right\}^{1/2}, \tag{18}$$

where the parameter r is given by

$$r = \frac{4\kappa\gamma_\perp}{(2\kappa+\gamma_\perp)^2}(1-N/N_{\rm th}).$$

For $r \ll 1$, as obtained for pumping levels where N is close to $N_{\rm th}$, we expand equation (18) as a series in r and to first order in r obtain

$$\gamma_{\rm las} \approx \frac{2\kappa+\gamma_\perp}{2}r = \gamma_c(1-N/N_{\rm th}), \tag{19}$$

where $\gamma_c = 2\kappa\gamma_\perp/(2\kappa+\gamma_\perp)$. Examples of optical spectra calculated according to equation (16) are given in figure 2, showing both cases of single- and double-peaked spectra.

Our goal in the remainder of this section is to express the linewidth $\gamma_{\rm las}$ in terms of familiar laser parameters. In order to do so we first determine the population inversion N. (Incidentally, the same procedure to calculate N will be used later again, when we also take population fluctuations into account.) From equations (13) and (16) we find for the mean number of photons in the cavity

$$n = \frac{\gamma_\perp N_e}{(2\kappa+\gamma_\perp)(N_{\rm th}-N)}. \tag{20}$$

By inserting this into the energy conservation law (4), we obtain a quadratic equation for the population inversion,

$$\tilde{\beta}_c(N_0+N) = [P(N_0-N)-N_0-N](1-N/N_{\rm th}), \tag{21}$$

where we introduced the parameters

$$\tilde{\beta}_c = \tilde{\beta}/(1+2\kappa/\gamma_\perp), \quad \text{with} \tag{22a}$$

$$\tilde{\beta} = 4\Omega_0^2 f/(\gamma_\perp\gamma_\parallel), \tag{22b}$$

following references [38, 60], respectively. In the special case $\tilde{\beta}_c = 0$ the two solutions of equation (21) for N coincide with the stationary population inversion found in semiclassical laser theory. The general solution of equation (21) with $\tilde{\beta}_c \neq 0$ is different, because the approach that led to equation (21) takes into account spontaneous emission into the lasing mode. Indeed, in the limit $2\kappa/\gamma_\perp \to 0$, the coefficient $\tilde{\beta}_c$ tends to $\tilde{\beta}$, which was introduced in reference [60] as the ratio of the rate of spontaneous emission into the lasing mode to the rate of all other emission processes (i.e. background emission).

We note that the Langevin force $\hat{F}_v$ in equation (10b) and in the equations below describes the polarisation fluctuations that are responsible for spontaneous emission into the lasing mode. In the limit $2\kappa/\gamma_\perp \to 0$ the solution (20) coincides with the solution of the laser rate equations derived in [60] where spontaneous emission into the lasing mode is taken into account. The derivation of the extended laser rate equations from equation (1) for arbitrary 2κ and $\gamma_\perp$ and including spontaneous emission into the lasing mode is given in [62]. The stationary solution of such extended rate equations coincides with equation (20).

Solving equation (21), we find the pump-dependent population inversion $N(P)$, given by equation (C1a) of appendix C. By inserting $N(P)$ into equation (18) we obtain an explicit expression for the pump-dependent linewidth $\gamma_{\rm las}(P)$. Similarly, by inserting $N(P)$ into the energy conservation law (4) we obtain the pump-dependent photon number $n(P)$, given in equation (C1b) of appendix C.

We can now express the linewidth (19) in terms of the laser output power $W_{\rm out} = 2\kappa\hbar\omega_0 n$ by using equation (20) to express the factor $(1 - N/N_{\rm th})$ in terms of $W_{\rm out}$, giving

$$\gamma_{\rm las} = \left(\frac{2\kappa\gamma_\perp}{2\kappa + \gamma_\perp}\right)^2 N_{\rm sp}\frac{\hbar\omega_0}{W_{\rm out}}, \tag{23}$$

where $N_{\rm sp} = N_e/N_{\rm th}$ is the so-called spontaneous-emission factor [64]. Equation (23) is the well-known result for the laser linewidth *below threshold*, which (apart from notations) coincides with, for example, results in references [57, 64].

It is generally accepted that the laser linewidth *far above threshold* is suppressed by a factor of two compared to equation (23) [57]. We notice, though, that recent work [65] challenges this result, based on a semiclassical analysis. In the next sections we will show that a fully quantum mechanical theory for the lineshape far above threshold agrees with adding the extra factor of $1/2$ to equation (23), and that it can be ascribed to the effect of population fluctuations, in particular to relaxation oscillations induced by population fluctuations.

4. Linearization of equations

Our aim is now to develop a theory for the optical spectrum applicable, in physically reasonable approximations, to lasers at any pump rate, without making the assumption that fluctuations in the lasing field and polarization are always small. Our linearization procedure is therefore, in some parts, different from the standard SSA as presented, for example, in references [36, 37, 54, 55]. We will try to clearly identify the approximations made.

We begin with the linearization of equation (1b) by writing the population operators as the sum of their mean values $N_{e,g}$ and population fluctuations $\delta\hat{N}_{e,g}$,

$$\hat{N}_{e,g} = N_{e,g} + \delta\hat{N}_{e,g}, \delta\hat{N}_g = -\delta\hat{N}_e, \tag{24}$$

whereby the population fluctuations are defined. We consider a large number $N_0 \gg 1$ of emitters and suppose small fluctuations of populations $\langle\delta\hat{N}^2_{e,g}\rangle^{1/2} \ll N_{e,g}$. We also suppose weak coupling, $2\Omega_0^2 f/\gamma_\perp\gamma_\parallel \ll 1$, and, for superradiant lasers, low-Q cavities with $2\kappa \geqslant \gamma_\perp$. The mean photon number for such a laser below and near the semiclassical threshold is of the order of unity or less, which we see in figure 4(a). So we do *not* assume that fluctuations of the lasing field and polarisation are small compared to their mean values.

We next insert equation (24) into equation (1) and obtain

$$\dot{\hat{a}} = -\kappa\hat{a} + \Omega_0\hat{v} + \hat{F}_a, \tag{25a}$$

$$\dot{\hat{v}} = -(\gamma_\perp/2)\hat{v} + \Omega_0 f\left(\hat{a}N + 2\hat{a}\delta\hat{N}_e\right) + \hat{F}_v, \tag{25b}$$

$$\delta\dot{\hat{N}}_e = -\Omega_0\left(\hat{v}^+\hat{a} + \hat{a}^+\hat{v} - \left\langle\hat{v}^+\hat{a} + \hat{a}^+\hat{v}\right\rangle\right) - \gamma_\parallel(P+1)\delta\hat{N}_e + \hat{F}_{N_e}. \tag{25c}$$

We shall now show that instead of the conventional representation of the laser field in terms of amplitude and phase, it is convenient to represent the field and polarization by their quadratures

$$\hat{\alpha}_x = (\hat{\alpha} + \hat{\alpha}^+)/\sqrt{2}, \qquad \hat{\alpha}_p = i(\hat{\alpha}^+ - \hat{\alpha})/\sqrt{2}, \tag{26}$$

where $\hat{\alpha}$ stands for $\hat{a}$ or $\hat{v}$. In our stochastic approach, $\hat{\alpha}_{x,p}$ are represented by real-valued stochastic variables. The equations of motion for the quadratures follow from equation (25),

$$\dot{\hat{a}}_{x,p} = -\kappa\hat{a}_{x,p} + \Omega_0\hat{v}_{x,p} + \hat{F}_{a_{x,p}}, \tag{27a}$$

$$\dot{\hat{v}}_{x,p} = -(\gamma_\perp/2)\hat{v}_{x,p} + \Omega_0 f\left(\hat{a}_{x,p}N + 2\hat{a}_{x,p}\delta\hat{N}_e\right) + \hat{F}_{v_{x,p}}, \tag{27b}$$

$$\delta\dot{\hat{N}}_e = -\Omega_0\left(\hat{a}_p\hat{v}_x + \hat{v}_p\hat{a}_x - \left\langle\hat{a}_p\hat{v}_x + \hat{v}_p\hat{a}_x\right\rangle\right) - \gamma_\parallel(P+1)\delta\hat{N}_e + \hat{F}_{N_e}. \tag{27c}$$

The Langevin forces in equations (27a) and (27b) are

$$\hat{F}_{\alpha_x} = (\hat{F}_\alpha + \hat{F}_{\alpha+})/\sqrt{2}, \qquad \hat{F}_{\alpha_p} = i(\hat{F}_{\alpha+} - \hat{F}_\alpha)/\sqrt{2},$$

where α stands for a or v.

Assume, at the beginning, a high pump rate of a laser. Well above threshold one can solve Maxwell–Bloch equation (27) approximately, by SSA similar to the approach in [54, 55]. In SSA, the

variables are replaced by the sums of large c-number parts and small time-dependent fluctuating parts. We already have seen such a replacement in equation (24) for $\hat{N}_{e,g}$. Now we similarly replace $\hat{a}_{x,p}$ and $\hat{v}_{x,p}$ by

$$\hat{a}^{\rm ssa}_{x,p}(t) = \sqrt{n} + \hat{a}'_{x,p} \tag{28a}$$

$$\hat{v}^{\rm ssa}_{x,p}(t) = V + \hat{v}'_{x,p}, \tag{28b}$$

where $\hat{a}'_{x,p}$, $\hat{v}'_{x,p}$ are the small fluctuations and the index ssa shows that the variables (28) correspond to the SSA.

We will use the SSA for MBE with care. Such SSA, just like the semiclassical solution of equation (5), assumes the phase of the coherent part of laser field to be constant. This is why $\left\langle \hat{a}^{\rm ssa}_{x,p} \right\rangle = \sqrt{n}$. By contrast, the solutions of equation (27) have vanishing statistical averages, $\left\langle \hat{a}_{x,p} \right\rangle = 0$—due to the phase diffusion, ignored by SSA of MBE. Phase diffusion cannot be ignored in our analysis. In particular, for high pump the phase diffusion determines the laser linewidth [33, 35, 36, 66]. So the SSA of MBE is unsuited to describe the optical spectrum and lineshape of a laser. This is why we will use the SSA only to linearize the nonlinear terms in equation (27), related with population fluctuations. As we will see, the SSA is good approach for calculations of population fluctuations.

The c-number $\sqrt{n}$ is chosen in equation (28a) in order to ensure that

$$\left(\left\langle (\hat{a}^{\rm ssa}_x)^2 \right\rangle + \left\langle (\hat{a}^{\rm ssa}_p)^2 \right\rangle \right)/2 \approx n, \tag{29}$$

where n is the mean number of photons in the laser cavity. In equation (29) we neglect the contribution of the commutation relation of $\hat{a}'_x$ and $\hat{a}'_p$ that is of order unity; we also neglect the small mean values of squares of fluctuations in the high-excitation limit ($n \gg 1$).

One may expect that in equation (28), different c-numbers should be defined for the different quadratures, instead of only $\sqrt{n}$ and V. However, the different c-numbers reduce to $\sqrt{n}$ and V by the replacements $\hat{a} \to \hat{a}\, e^{i\varphi}$ and $\hat{v} \to \hat{v}\, e^{i\varphi}$ with real-valued phase φ, which is the constant phase of the lasing field. The solution of the initial MBE (1) does not depend on such a replacement, which adds only a constant phase multiplier to the Langevin forces $\hat{F}_a$ and $\hat{F}_v$. Therefore $\sqrt{n}$ and V in equation (28) can be chosen to be the same for both quadratures x and p in the general case.

In the standard SSA we replace $\hat{a}_{x,p}$ and $\hat{v}_{x,p}$ by $\hat{a}^{\rm ssa}_x$ and $\hat{v}^{\rm ssa}_x$ in equation (27), where we neglect small nonlinear terms quadratic in the fluctuations; we then separate the stationary equations for $\sqrt{n}$, V (they are equations of the semiclassical laser theory) from the equations for fluctuations. From the stationary semiclassical laser equations we find

$$V = (\kappa/\Omega_0)\sqrt{n}. \tag{30}$$

Next, we solve linear equations for the fluctuations, find expressions for $\hat{a}'_x$ and $\hat{a}'_p$ and determine the laser field in the SSA approximation (28). This approximation does not suffice for calculating optical spectra and the laser linewidth, because it entails that the narrow lasing peak in the optical spectrum is replaced by a delta-function of zero width in frequency space.

As announced above, in order to find optical spectra and the laser linewidth from analytically solvable linear equations, we modify the standard SSA procedure: we replace $\hat{a}_{x,p}$ and $\hat{v}_{x,p}$ by $\hat{a}^{\rm ssa}_{x,p}$ and $\hat{v}^{\rm ssa}_{x,p}$ not everywhere in equation (27), but only in the nonlinear terms $2\Omega_0 f \hat{a}_{x,p}\delta\hat{N}_e$ and $-\Omega_0\left(\hat{a}_p\hat{v}_x + \hat{v}_p\hat{a}_x - \left\langle \hat{a}_p\hat{v}_x + \hat{v}_p\hat{a}_x \right\rangle\right)$. After this we neglect the small products of fluctuations in these terms, as in the standard SSA, and obtain the linear equations for the quadratures

$$\dot{\hat{a}}_{x,p} = -\kappa\hat{a}_{x,p} + \Omega_0\hat{v}_{x,p} + \hat{F}_{a_{x,p}}, \tag{31a}$$

$$\dot{\hat{v}}_{x,p} = -(\gamma_\perp/2)\hat{v}_{x,p} + \Omega_0 f\left(\hat{a}_{x,p}N + 2\sqrt{n}\delta\hat{N}_e\right) + \hat{F}_{v_{x,p}}, \tag{31b}$$

and for the population fluctuations

$$\delta\dot{\hat{N}}_e = -\Omega_0\left[\sqrt{n}(\hat{v}'_x + \hat{v}'_p) + V(\hat{a}'_x + \hat{a}'_p)\right] - \gamma_\parallel(P+1)\delta\hat{N}_e + \hat{F}_{N_e}. \tag{32}$$

Equation (31) are for fluctuating quadratures with zero mean. We will see that the spectrum found with the $\hat{a}_{x,p}$ solutions of equation (31) does not feature a delta-function, but rather a narrow peak of finite width.

In the standard SSA, the variables $\sqrt{n}$ and N at high excitation are solutions of the semiclassical laser equations. In contrast to the standard SSA, we do not know exactly the n and N in equations (31) and (32).

Below we calculate n and N using a solution of equations (31) and (32), similar to our calculation of the unknown N in equation (10) of section 3. The fact that n and N are determined by the fluctuating laser field, polarization and populations make our approach different from the standard SSA. This lets us find

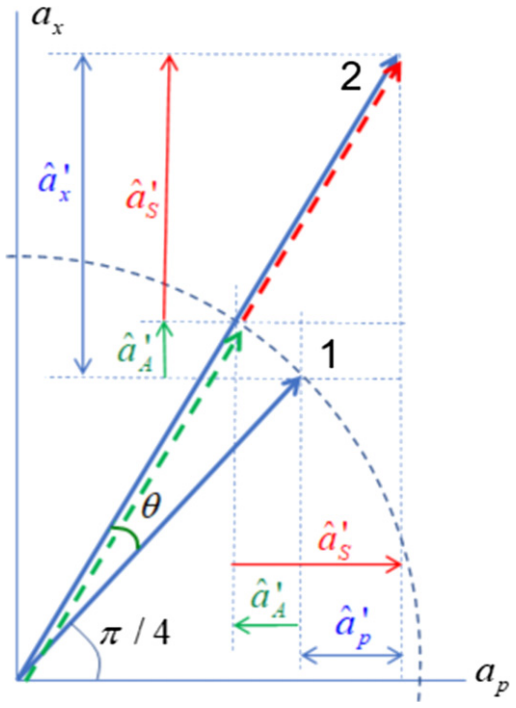

Figure 3. Sketch of the lasing field and its fluctuations. The initial lasing field, represented by the blue vector 1 at an angle of 45°, changes into vector 2 due to a fluctuation of its direction and length during a short time Δt much smaller than the characteristic time scale for direction (phase) fluctuations $\gamma_{\rm las}^{-1}$. Direction fluctuations are much slower than length fluctuations, so after Δt the difference angle $\theta \ll 1$. Also shown are the quadratures $\hat{a}'_{x,p}$ as well as the symmetric $\hat{a}'_{\rm S}$ and anti-symmetric $\hat{a}'_{\rm A}$ combinations that are defined by equation (34) and used in the approximation (28). The identities $\hat{a}'_x = \hat{a}'_{\rm S} + \hat{a}'_{\rm A}$ and $\hat{a}'_p = \hat{a}'_{\rm S} - \hat{a}'_{\rm A}$ explain why $\hat{a}'_{\rm A,S}$ (see red and green arrows) are illustrated along both axes. For $\theta \ll 1$, the $\hat{a}'_{\rm S}$ and $\hat{a}'_{\rm A}$ combinations determine, correspondingly, the amplitude and phase fluctuations of the field. The green (the red) dashed vectors denote the change of the field vector 1 due to only phase (amplitude) fluctuations.

$n \neq 0$, N as well as optical spectra at low excitation, similar to section 3, but now also taking population fluctuations into account.

Equation (32) for $\delta\hat{N}_e$ depends on fluctuations of the quadratures $\hat{a}'_{x,p}$ and $\hat{v}'_{x,p}$ as introduced in equation (28). The equations for $\hat{a}'_{x,p}$ and $\hat{v}'_{x,p}$ can be found by the standard SSA procedure: we insert the approximation (28) everywhere into equation (25), neglect the small terms that are quadratic in the fluctuations and write linear equations for the fluctuations as

$$\dot{\hat{a}}'_{x,p} = -\kappa\hat{a}'_{x,p} + \Omega_0\hat{v}'_{x,p} + \hat{F}_{a_{x,p}}, \tag{33a}$$

$$\dot{\hat{v}}'_{x,p} = -(\gamma_\perp/2)\hat{v}'_{x,p} + \Omega_0 f\left(\hat{a}'_{x,p}N + 2\sqrt{n}\delta\hat{N}_e\right) + \hat{F}_{v_{x,p}}. \tag{33b}$$

Together with equation (32) this constitutes a closed set of equations for $\delta\hat{N}_e$. We insert its solution into the linear equation (31) for the quadratures, solve these equations and end up with solutions for $\hat{a}_{x,p}$ and $\hat{v}_{x,p}$.

It is convenient to carry out calculations by extracting the symmetric (S) $\hat{\alpha}_{\rm S}$ and anti-symmetric (A) $\hat{\alpha}_{\rm A}$ combinations of the quadratures and their fluctuations introduced in (28)

$$\begin{aligned} \hat{\alpha}_{\rm S} &= (\hat{\alpha}_x + \hat{\alpha}_p)/2, \qquad & \hat{\alpha}_{\rm A} &= (\hat{\alpha}_x - \hat{\alpha}_p)/2, \\ \hat{\alpha}'_{\rm S} &= (\hat{\alpha}'_x + \hat{\alpha}'_p)/2, \qquad & \hat{\alpha}'_{\rm A} &= (\hat{\alpha}'_x - \hat{\alpha}'_p)/2, \end{aligned} \tag{34}$$

where α means a or v. A-combinations change their signs upon exchange of the indices $x \rightleftarrows p$ in equation (34), while S-combinations do not. From the inverse relations $\hat{\alpha}'_x = \hat{\alpha}'_{\rm S} + \hat{\alpha}'_{\rm A}$ and $\hat{\alpha}'_p = \hat{\alpha}'_{\rm S} - \hat{\alpha}'_{\rm A}$, we see that S-combinations contribute in the same way to the x- and p-quadratures, whereas A-combinations contribute with the same absolute values to both quadratures, but with opposite signs. These properties lead to the important physical interpretation that *S-combinations correspond to amplitude fluctuations while A-combinations correspond to phase fluctuations*, as illustrated in figure 3.

We obtain four linear equations for the S- and A-combinations of quadratures from equations (31) and (34)

$$\dot{\hat{a}}_{\rm A,S} = -\kappa\hat{a}_{\rm A,S} + \Omega_0\hat{v}_{\rm A,S} + \hat{F}_{a_{\rm A,S}}, \tag{35a}$$

$$\dot{\hat{v}}_{\rm A} = -(\gamma_\perp/2)\hat{v}_{\rm A} - \Omega_0 f\hat{a}_{\rm A}\,(2N_e - N_0) + \hat{F}_{v_{\rm A}}, \tag{35b}$$

$$\dot{\hat{v}}_{\rm S} = -(\gamma_\perp/2)\hat{v}_{\rm S} + \Omega_0 f\left[\hat{a}_{\rm S}\,(2N_e - N_0) + 2\sqrt{n}\delta\hat{N}_e\right] + \hat{F}_{v_{\rm S}}, \tag{35c}$$

and three equations for symmetric combinations of quadrature fluctuations in the SSA approximation introduced in equations (28) and (34), and for $\delta\hat{N}_e$

$$\dot{\hat{a}}'_{\rm S} = -\kappa\hat{a}'_{\rm S} + \Omega_0\hat{v}'_{\rm S} + \hat{F}_{a_{\rm S}}, \tag{36a}$$

$$\dot{\hat{v}}'_{\rm S} = -(\gamma_\perp/2)\hat{v}'_{\rm S} + \Omega_0 f\left[\hat{a}'_{\rm S}\,(2N_e - N_0) + 2\sqrt{n}\delta\hat{N}_e\right] + \hat{F}_{v_{\rm S}}, \tag{36b}$$

$$\delta\dot{\hat{N}}_e = -2\sqrt{n}\left(\Omega_0\hat{v}'_{\rm S} + \kappa\hat{a}'_{\rm S}\right) - \gamma_\parallel(P+1)\delta\hat{N}_e + \hat{F}_{N_e}, \tag{36c}$$

with

$$\hat{F}_{\alpha_{\rm S,A}} = (\hat{F}_\alpha\,{\rm e}^{\mp{\rm i}\pi/4} + \hat{F}_{\alpha^+}\,{\rm e}^{\pm{\rm i}\pi/4})/2, \tag{37}$$

and where α stands for a or v.

We see that equation (35) are split into two sets of equations: the two equations (35a) and (35b) for the A-combinations of the quadratures, and the five equations: (35a) and (35c) for S-combinations of quadratures, two equations (36a) and (36b) for S-combinations of fluctuations of quadratures in the SSA approximation introduced in equation (28b), and equation (36c) for $\delta\hat{N}_e$.

We now find $\delta\hat{N}_e$ by solving the set of equation (36), then substitute this $\delta\hat{N}_e$ into equation (35) and solve equation (35). This straightforward but cumbersome procedure can be simplified by noting that the fluctuations $\hat{a}'_{\rm S}$ and $\hat{v}'_{\rm S}$ of S-combinations of quadratures in SSA approximation coincide with $\hat{a}_{\rm S}$ and $\hat{v}_{\rm S}$—solutions of equation (35). Indeed, equations (36a) and (36b) for $\hat{a}'_{\rm S}$ and $\hat{v}'_{\rm S}$ are the same as equations (35a) and (35c) for $\hat{a}_{\rm S}$ and $\hat{v}_{\rm S}$. Therefore $\hat{a}'_{\rm S}$ and $\hat{v}'_{\rm S}$ differ from $\hat{a}_{\rm S}$ and $\hat{v}_{\rm S}$ only by constant parts. But $\hat{a}'_{\rm S}$, $\hat{v}'_{\rm S}$, $\hat{a}_{\rm S}$ and $\hat{v}_{\rm S}$ have zero means by definition, so such constant parts must be zero for all of them. We obtain, of course, the same $\delta\hat{N}_e$ from equation (36c) with $\hat{a}'_{\rm S}$ and $\hat{v}'_{\rm S}$, or if we replace in equation (36c) $\hat{a}'_{\rm S}$ and $\hat{v}'_{\rm S}$ by $\hat{a}_{\rm S}$ and $\hat{v}_{\rm S}$ found from equations (35a) and (35c). So in equation (36) we can replace the fluctuations $\hat{a}'_{\rm S}$ and $\hat{v}'_{\rm S}$ introduced in the SSA by the symmetric combinations $\hat{a}_{\rm S}$ and $\hat{v}_{\rm S}$ which we are looking for. And we obtain the final set of linear equations

$$\dot{\hat{a}}_{\rm A,S} = -\kappa\hat{a}_{\rm A,S} + \Omega_0\hat{v}_{\rm A,S} + \hat{F}_{a_{\rm A,S}}, \tag{38a}$$

$$\dot{\hat{v}}_{\rm A} = -(\gamma_\perp/2)\hat{v}_{\rm A} - \Omega_0 f\hat{a}_{\rm A}\,(2N_e - N_0) + \hat{F}_{v_{\rm A}}, \tag{38b}$$

$$\dot{\hat{v}}_{\rm S} = -(\gamma_\perp/2)\hat{v}_{\rm S} + \Omega_0 f\left[\hat{a}_{\rm S}\,(2N_e - N_0) + 2\sqrt{n}\delta\hat{N}_e\right] + \hat{F}_{v_{\rm S}}, \tag{38c}$$

$$\delta\dot{\hat{N}}_e = -2\sqrt{n}\,(\Omega_0\hat{v}_{\rm S} + \kappa\hat{a}_{\rm S}) - \gamma_\parallel(P+1)\delta\hat{N}_e + \hat{F}_{N_e}. \tag{38d}$$

The five equation (38) are split into two sets of equations: the first—for $\hat{a}_{\rm A}$ and $\hat{v}_{\rm A}$ and the second—for $\hat{a}_{\rm S}$, $\hat{v}_{\rm S}$ and $\delta\hat{N}_e$. They will lead to the same results as the set of seven equations (35) and (36) (not shown).

In order to find the mean photon number n, we express

$$\hat{a} = \hat{a}_{\rm S}\,{\rm e}^{{\rm i}\pi/4} + \hat{a}_{\rm A}\,{\rm e}^{-{\rm i}\pi/4}, \tag{39}$$

insert this equation (39) into $n = \langle\hat{a}^+\hat{a}\rangle$ and obtain

$$n = n_{\rm S}(N_e) + n_{\rm A}(N_e) + i\,\langle[\hat{a}_{\rm A}, \hat{a}_{\rm S}]\rangle\,. \tag{40}$$

Inserting equation (39) into $[\hat{a}, \hat{a}^+] = 1$ we find $[\hat{a}_{\rm A}, \hat{a}_{\rm S}] = i/2$, while for the mean photon number we obtain

$$n = n_{\rm S}(N_e) + n_{\rm A}(N_e) - 1/2. \tag{41}$$

By inserting this equation (41) into the energy conservation law (4), we obtain an equation for N_e.

We will make some remarks about equation (38) and about their applicability.

Solving equation (38) we will see that $\langle\hat{a}^2_{\rm S}\rangle \ll \langle\hat{a}^2_{\rm A}\rangle$ for strong pumping (see the discussion after equation (49)). In order to preserve this last inequality in the SSA, we must replace the solution of equation (38) by

$$\hat{a}^{\rm ssa}_x = \sqrt{n} + \hat{a}'_x, \qquad \hat{a}^{\rm ssa}_p = -\sqrt{n} + \hat{a}'_p, \tag{42}$$

(and similar for $\hat{v}_{x,p}$). Then

$$\langle\hat{a}^2_{\rm S}\rangle = \langle(\hat{a}'_x + \hat{a}'_p)^2\rangle/4 \ll \langle\hat{a}^2_{\rm A}\rangle = \langle(\hat{a}'_x - \hat{a}'_p)^2\rangle/4 \approx n.$$

The SSA replacement (42) differs by the sign of the c-number term for $\hat{a}^{\rm ssa}_p$ (and similarly for $\hat{v}^{\rm ssa}_p$) from the SSA replacement (28). This means that the field and polarisation found from equation (38) in SSA both

have constant phase shifts of $\pi/2$ with respect to the ones used in the SSA replacement (28). This difference is insignificant, because a constant phase of the field and polarisation, introduced in the equation for $\delta\hat{N}_e$, does not affect the results. Suppose that we solved the exact equation (1) numerically, so that we found $\hat{a}$ and $\hat{v}$. If we then would add a constant phase φ to both of them, by introducing $\hat{a}_\varphi = \hat{a}\,e^{i\varphi}$, $\hat{v}_\varphi = \hat{v}\,e^{i\varphi}$, and replacing $\hat{a}$ and $\hat{v}$ by $\hat{a}_\varphi$ and $\hat{v}_\varphi$ in equation (1c), we would obtain

$$\dot{\hat{N}}_e = -\Omega_0(\hat{a}_\varphi^+\hat{v}_\varphi + \hat{v}_\varphi^+\hat{a}_\varphi) + \gamma_\parallel(P\hat{N}_g - \hat{N}_e) + \hat{F}_{N_e} \tag{43}$$

from which $\hat{N}_e$ can be found (numerically). The result for $\hat{N}_e$ will obviously be the same as obtained from the original equation (1), since the phase factor $e^{i\varphi}$ in $\hat{a}_\varphi$ and $\hat{v}_\varphi$, is canceled in equation (43).

When the pump is diminished, population fluctuations also decrease, and the solution of equation (38) gradually approaches the solution of equation (10) found without population fluctuations. Then it is natural to use equation (38) also for moderate and for low excitations. We leave a rigorous justification of equation (38) for low excitations for the future, but here instead provide some physical arguments for the applicability of equation (38) at moderate and low excitations.

The largest error at low excitation comes from the first term in equation (38d) for population fluctuations, because in this term we neglect second-order correlations (shown explicitly in equation (27c)) that are not necessarily small at low excitation. However, this term only makes a broadband contribution of width $\sim\gamma_\perp$. When considering the effect of this first term, while omitting the second term, we find that the first term does not introduce any specific features in the spectra at low excitation. In other words, the first term in equation (38d) gives only a small change in the *spectral power density* everywhere in the spectrum.

By contrast, the influence of the second term of equation (38d), $\sim\gamma_\parallel$, on the optical spectra is concentrated in the narrow spectral region $\sim\gamma_\parallel \ll \gamma_\perp$ near zero frequency, where it competes with the first term and produces interesting features such as a peak or a dip in spectra near $\omega = 0$, as we will see. So we will use equation (38) also at moderate and low excitations. We will keep all terms in equation (38d) in order to provide the correct asymptotic behavior at high excitations and it will turn out that new features related to population fluctuations appear for weak pumping.

Equations (38a) and (38b) for the A-combinations do not depend on population fluctuations explicitly and can be solved independently from the rest of equation (38). However, the A-combinations do depend on n_S and, therefore, on $\delta\hat{N}_e$ implicitly, through the energy conservation law (4), where $n(N_e)$ is given by equation (41). Because of this, we will obtain different relations between n_A, n_S and n at low and at high excitations.

5. Solving the combinations of the field quadratures

In this section we first solve the equations (38a) and (38b) for the A-combinations of the field and polarization quadratures, these equations being the ones that do not explicitly depend on population fluctuations. In doing so, well-known results for the laser linewidth in the high-pump limit will be reproduced.

We replace $\hat{a}_A$ and $\hat{v}_A$ in equations (38a) and (38b) by their Fourier expansions (11), then solve the linear equations for the Fourier components $\hat{a}_A(\omega)$ and $\hat{v}_A(\omega)$, and find

$$\hat{a}_A(\omega) = \frac{(\gamma_\perp/2 - i\omega)\hat{F}_{a_A}(\omega) + \Omega_0\hat{F}_{v_A}(\omega)}{(i\omega - \kappa)\left(i\omega - \gamma_\perp/2\right) - \Omega_0^2 fN}. \tag{44}$$

From $\hat{a}_A(\omega)$ we can calculate the corresponding optical spectrum $n_A(\omega)$ by

$$\langle\hat{a}_A(\omega)\hat{a}_A(\omega')\rangle = n_A(\omega)\delta(\omega + \omega'), \tag{45}$$

analogous to equation (14). The relevant diffusion coefficients are given by

$$2D_{a_Aa_A} = \kappa/2, 2D_{v_Av_A} = f\gamma_\perp N_0/4, \tag{46}$$

as calculated in appendix B. With the help of equation (44), the diffusion coefficients (46), and the correlations of Langevin forces (2), we find the spectrum of the A-combinations of the photon field to be

$$n_A(\omega) = \frac{(\kappa/2)[(1 + N_0/N_{th})\gamma_\perp^2/4 + \omega^2]}{[(1 - N/N_{th})(\kappa\gamma_\perp/2) - \omega^2]^2 + \omega^2(\kappa + \gamma_\perp/2)^2}. \tag{47}$$

The photon numbers $n_{A,S}$ residing in the A- or S-combinations are in general given by the integrated spectra

$$n_{A,S} = \frac{1}{2\pi}\int_{-\infty}^{\infty} n_{A,S}(\omega)\mathrm{d}\omega. \tag{48}$$

By carrying out this integration with $n_A(\omega)$ given by equation (47), we find the number of photons in the A-combinations of the field quadratures as

$$n_A = \frac{\gamma_\perp}{4(2\kappa+\gamma_\perp)}\left(\frac{N_0+N_{th}}{N_{th}-N}+\frac{2\kappa}{\gamma_\perp}\right). \tag{49}$$

So here we find, perhaps not surprisingly, that n_A can grow very large when the laser is pumped strongly and the population inversion N approaches its semiclassical stationary value N_{th}. However, in section 6 we will see that in the same high-pump limit, the number of photons n_S in the S-combinations of the quadratures is much smaller than n_A in equation (49). Mathematically, this is the case because n_S does not have a corresponding term $\sim 1/(N_{th}-N)$. Physically, because n_S is suppressed by relaxation oscillations introduced by population fluctuations. So almost all lasing photons reside in the A-combinations and $n_A \approx n$. Anticipating these results for the spectra and for the number of photons in the A-combinations, we now replace n_A by n in equation (49), and use this to derive an expression for the linewidth as a function of the laser output power, as we did before in equation (23): in equation (49) we neglect the term $2\kappa/\gamma_\perp$, which above threshold is small compared to the large first term $\propto (N_{th}-N)^{-1}$. The linewidth γ_{las} is again defined as the full width at half maximum of the optical spectrum, i.e. $n_A(\gamma_{las}/2) = n_A(\omega=0)/2$. This leads to exactly the same expressions (18) and (19) for the linewidth γ_{las} as found previously for the spectrum (16), when expressed in terms of the average population inversion, N. However, the crucial difference is that the variation of N with the pump level P changes quantitatively as the laser threshold is passed, leading to different dependencies of the laser linewidth on power above and below the laser threshold.

To see this, we express $(N_{th}-N)$ in terms of n and the laser output power W_{out}. We insert the result into equation (19), and obtain for the *laser linewidth in the high-excitation limit*

$$\gamma_{las} = \frac{1}{2}\left(\frac{2\kappa\gamma_\perp}{2\kappa+\gamma_\perp}\right)^2 N_{sp}\frac{\hbar\omega_0}{W_{out}}. \tag{50}$$

This looks a lot like equation (23) for the laser linewidth in the *low-pump limit*. It differs only by the prefactor of $1/2$ in equation (50), and by a different expression for the spontaneous-emission factor, which for equation (50) reads

$$N_{sp} = (N_0+N_{th})/2N_{th}. \tag{51}$$

The result (50) is the same as, for example, in reference [67]. Our approach gives a new interpretation to this remarkable result: the linewidths (23) and (50) at low and at high pump rates are different due the different roles of population fluctuations below and above threshold. As shown in the next section, above threshold the population fluctuations reduce the number of photons in S- and increase it in A-combinations, which govern only slow frequency fluctuations and thereby narrow the linewidth. We will also see that the total number of photons $n(P)$ in the field practically does not depend on population fluctuations.

6. Calculation and analysis of optical spectra

Equations (38a) and (38c) for the symmetric combinations $\hat{a}_S$ and $\hat{v}_S$ of the field and polarization and equation (38d) for population fluctuations lead to algebraic equations for the Fourier-component operators $\hat{a}_S(\omega)$, $\hat{v}_S(\omega)$, and $\delta\hat{N}_e(\omega)$. By solving them, we obtain the Fourier-component $\hat{a}_S(\omega)$ of the S-combinations of the field quadratures. Then, using relation (45) with indices 'S' instead of 'A', we find the spectrum of the S-combinations as

$$n_S(\omega) = \frac{\kappa[(\omega_{ro}^2-\omega^2+\gamma_P\gamma_\perp/2)^2+\omega^2(\gamma_\perp/2+\gamma_P)^2]+\kappa\gamma_\perp^2(\omega^2+\gamma_P^2)N_0/4N_{th}+\omega_{ro}^2\kappa\gamma_\parallel\gamma_\perp(PN_g+N_e)/N_{th}}{2|(i\omega-\gamma_P)[(1-N/N_{th})\kappa\gamma_\perp/2-\omega^2-i\omega(\kappa+\gamma_\perp/2)]+\omega_{ro}^2(i\omega-2\kappa)|^2}, \tag{52}$$

where $\gamma_P \equiv \gamma_\parallel(P+1)$ and

$$\omega_{ro}^2 \equiv 4\Omega_0^2 fn \tag{53}$$

is the squared relaxation oscillation frequency at high pump in the rate-equation limit $2\kappa \ll \gamma_\perp$ [37]. For the derivation of equation (52) we used the diffusion coefficients $2D_{a_Sa_S} = 2D_{a_Aa_A}$ and $2D_{v_Sv_S} = 2D_{v_Av_A}$

given by equation (46), and the diffusion coefficient

$$2D_{N_eN_e} = \gamma_{\parallel}(PN_g + N_e). \tag{54}$$

We have found that correlations between the Langevin forces representing fluctuations of the carrier population and the polarization give only a very small contribution to the spectrum for a large number of emitters $N_0 \gg 1$ and at weak coupling $\Omega_0/(2\kappa + \gamma_\perp) \ll 1$, which is the case considered here. For that reason we shall in the following neglect these correlations and put the corresponding diffusion coefficients to zero (i.e. $2D_{v_{A,S}N_e} = 0$).

The full spectrum of the lasing mode is

$$n(\omega) = n_A(\omega) + n_S(\omega) + n_{AS}(\omega), \tag{55}$$

where $n_A(\omega)$ and $n_S(\omega)$ are given by equations (47) and (52). So we are left with calculating $n_{AS}(\omega)$. By inserting the Fourier expansions (11) for $\hat{a}_S$ and $\hat{a}_A$ into the commutator $\langle[\hat{a}_A, \hat{a}_S]\rangle$ in equation (40), we find for $n_{AS}(\omega)$ the relation

$$i\langle[\hat{a}_A(\omega), \hat{a}_S(\omega')]\rangle = n_{AS}(\omega)\delta(\omega + \omega').$$

We find $n_{AS}(\omega)$ approximately, by neglecting the small population fluctuations. This way we automatically satisfy the commutation relation $(2\pi)^{-1}\int_{-\infty}^{\infty} n_{AS}(\omega)\mathrm{d}\omega = -1/2$. It is not easy to satisfy these commutation relations, when taking population fluctuations into account, as shown for example in appendix B. We leave for the future the problem of preserving commutation relations while taking population fluctuations into account.

By setting $\delta\hat{N}_e = 0$ (that is the case considered in section 3) in equation (35), we see that the equations for $\hat{a}_S$ and $\hat{v}_S$ are identical to the equations for $\hat{a}_A$ and $\hat{v}_A$, so that $n_A(\omega) = n_S(\omega)$ and therefore

$$n_{AS}(\omega) \approx 2n_A(\omega) - n(\omega)|_{\delta\hat{N}_e=0}, \tag{56}$$

where $n(\omega)|_{\delta\hat{N}_e=0}$ is obtained in section 3 and given by equation (16). By inserting equation (56) into equation (55) and applying there equations (16) and (47), we obtain the lasing spectrum

$$n(\omega) = n_S(\omega) + \frac{(\kappa\gamma_\perp^2/4N_{th})(N + N_0/2) - 0.5\kappa(\gamma_\perp^2/4 + \omega^2)}{[(1 - N/N_{th})(\kappa\gamma_\perp/2) - \omega^2]^2 + \omega^2(\kappa + \gamma_\perp/2)^2}, \tag{57}$$

with $n_S(\omega)$ still given by equation (52).

The spectrum $n(\omega)$ depends on the population inversion N, which can be found from the energy conservation law (4) in the same way as in section 3. We express n [entering $n_S(\omega)$ through equation (53)] through N by the same energy conservation law (4). Then, the population inversion N is the only unknown variable in equation (4). Written in terms of the numbers of photons in the S- and A-combinations, the conservation law becomes

$$n_S(N) + n_A(N) - 1/2 = \frac{\gamma_\parallel}{4\kappa}[P(N_0 - N) - N_0 - N]. \tag{58}$$

Here, $n_A(N)$ is given by equation (49), and $n_S(N)$ is found by integrating equation (48) with $n_S(\omega)$ given by equation (52). We find the mean population inversion N by solving the integral equation (58) numerically.

In our calculation examples we choose parameters close to typical ones for photonic crystal nanolasers with quantum-dot active media [38]: for the wavelength of the lasing transition we pick $\lambda_0 = 1.55\ \mu$m, for the background refractive index $n_r = 3.3$, the cavity mode volume $V_c = 10(\lambda_0/n_r)^3$ with $N_0 = 100$ emitters; a population relaxation rate $\gamma_\parallel = 10^9\ \mathrm{s}^{-1}$; a vacuum Rabi frequency $\Omega_0 = (d/n_r)[\omega_0/(\varepsilon_0\hbar V_c)]^{1/2}$ with a dipole moment of the lasing transition $d = 10^{-28}$ cm so that $\Omega_0 = 34\gamma_\parallel$; the average atom-lasing mode-coupling factor $f = 1/2$; finally, we choose the cavity quality factor $Q = 1.2 \times 10^4$ so that $2\kappa = 100\gamma_\parallel$.

In the examples below we vary the dephasing rate $\gamma_\perp$ and the pump P while keeping all other parameters fixed. The value for $\gamma_\perp$ is varied between $\gamma_\perp^{\min} = 50$ GHz (so that $2\kappa/\gamma_\perp^{\min} = 2$) to $\gamma_\perp^{\max} = 1.5$ THz (with $2\kappa/\gamma_\perp^{\max} = 0.07$). This is a realistic region of $\gamma_\perp$ for quantum dots [68]. Within this range for $\gamma_\perp$, the conventional beta-factor β varies from 0.98 to 0.6, while the beta-factor $\tilde{\beta}_c$ varies from 15 to 1.4, so lasers with the chosen parameters have significant amounts of spontaneous emission into the lasing mode.

Lasers with high β-factors and low dephasing rates, $2\kappa/\gamma_\perp^{\min} = 2$, are superradiant, while lasers with $2\kappa/\gamma_\perp^{\max} = 0.07 \ll 1$ are not superradiant even if $\tilde{\beta}_c > 1$. Upon variation of $\gamma_\perp$ between $\gamma_\perp^{\min}$ and $\gamma_\perp^{\max}$, we will thus be able to compare results for superradiant and for non-superradiant lasers.

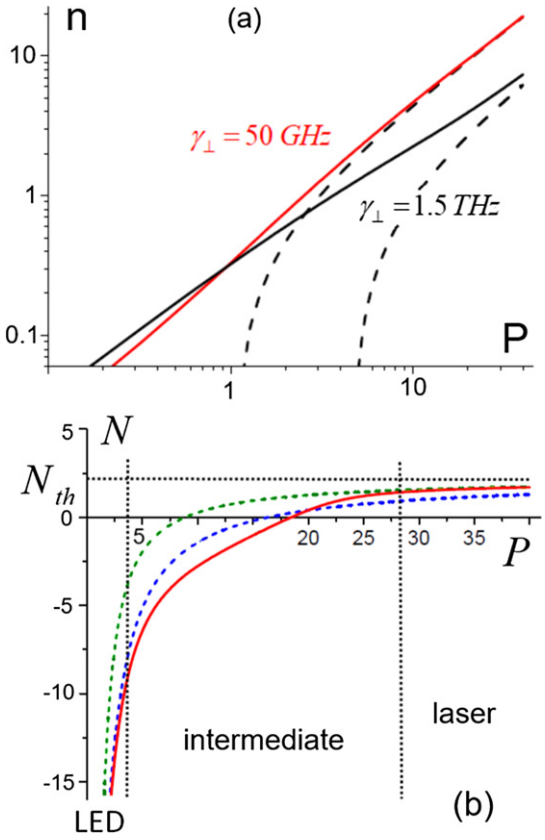

Figure 4. (a) Mean photon number for a superradiant laser with $\gamma_\perp^{\min} = 50$ GHz (red curve) and for a non-superradiant laser with $\gamma_\perp^{\max} = 1.5$ THz (black curve). Black dashed curves are $n(P)$ as calculated by the semiclassical model of equation (5). (b) Population inversion $N(P)$ for superradiant laser (red curve). Green (blue) dashed curves show the asymptotics of $N(P)$ at high (low) pump. The green curve is $N(P)$ at $n = n_A$ for large pump; the blue curve is $N(P)$ without population fluctuations. Vertical dotted lines separate the LED and laser regions from an intermediate cross-over region.

6.1. Photon numbers and population inversions

Calculations of mean values of photon numbers and population inversions are helpful for the identification of different lasing regimes and for understanding the role of population fluctuations. Our procedure to find the mean photon numbers and population inversions is as follows: first we calculate $n_S(N)$ by inserting the spectrum $n_S(\omega)$ from equation (52) into equation (48). Then we insert $n_S(N)$ found from equation (48) and $n_A(N)$ from equation (49) into the energy conservation law (58). By solving the latter equation, we can determine the population inversion N. By inserting this N back into $n_{S,A}(N)$, we find the mean photon number n from equation (41).

The red curve in figure 4(a) shows the mean photon number $n(P)$ for a superradiant laser, while the corresponding black curve is for a non-superradiant laser. For low pump rates the superradiant laser exhibits 'subradiance' and excitation trapping [22, 24], i.e. the photon number is smaller than for a non-superradiant laser. At high pump rates, by contrast, the superradiant laser is seen to generate more photons than the non-superradiant laser. There are two reasons for this: first, excitation trapping becomes weaker as the average emitter population grows and is suppressed when population inversion is achieved; second, in our case the superradiant laser has a smaller polarization relaxation rate $\gamma_\perp$ than the non-superradiant laser.

Panel figure 4(b) shows the population inversion $N(P)$ for a superradiant laser (red curve). The blue dashed curve depicts $N(P)$ as found by neglecting population fluctuations, which should be a good approximation for low pump rates. The dashed green curve shows $N(P)$ in the approximation $n \approx n_A$, which should be valid for high pump rates. The exact red curve indeed approaches the blue (green) curves at low (high) pump rates.

By following the red curve in figure 4(b) and observing where it approaches its asymptotics at low and at high pump rates, we can roughy identify three regions: the LED region at small pump rates, where fluctuations of populations are negligible; the lasing region at high pump rates, when almost all photons reside in the A-combinations of quadratures; and the remaining intermediate region between the lasing and the LED regions. These regions are separated by vertical dotted lines in figure 4(b).

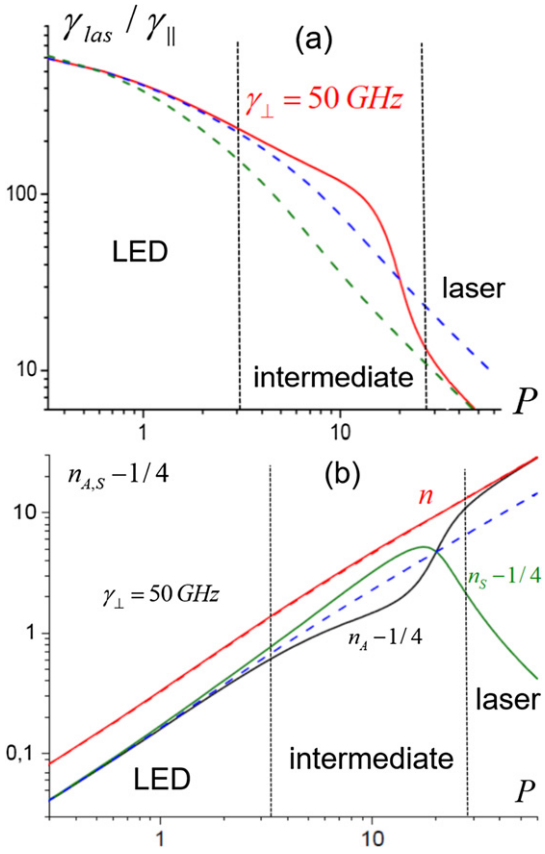

Figure 5. (a) Linewidth $\gamma_{las}(P)$ of equation (18) for a superradiant laser with $\gamma_\perp = 50$ GHz, with N found from equation (58) (red curve). An approximation for $\gamma_{las}(P)$ in the low-pump limit is obtained by neglecting population fluctuations (dashed blue curve) and in the high-pump limit (dashed green curve), with N given by equation (C1a) for both these limits; (b) photon numbers in the S- (green curve) and A-combinations (black curve) of the field of a superradiant laser. The same three radiation regions as in figure 4(b) are shown, separated by vertical dotted lines. The red line is the mean photon number n (41), which practically overlaps the red dotted line depicting n without population fluctuations.

Figure 5(a) shows the linewidth $\gamma_{las}(P)$, given by equation (18) with N determined from equation (58) for a superradiant laser (red curve). The LED, intermediate and lasing regions shown in figure 5 are the same as found in figure 4(b). The effects of the same approximations as in figure 4 are now shown for the linewidth: the blue dashed curve in figure 5(a), given by equation (23) for a laser below threshold [57, 64], represents the approximation of neglecting population fluctuations, which is again shown to be valid for small pump rates, i.e. in the LED region. The green dashed curve in figure 5(a) is given by the laser linewidth equation (50) for a laser far above threshold [67] that was found by taking $n \approx n_A$. As before in figure 4, this approximation is shown to be accurate at large pump rates, i.e. in the lasing region.

Figure 5(b) shows the photon numbers $(n_{S,A} - 1/4)$ of the S- and A-combinations of the field quadratures for a superradiant laser. The reason to display $(n_{S,A} - 1/4)$ on the vertical logarithmic axis is that in the low-pump limit $P \to 0$, when $n_S \to n_A$, we have $n_{S,A} \to 1/4$, in accordance with equation (58). We see that population fluctuations (from now on abbreviated as PF) have different influences on n_S and n_A. Removing $\delta\hat{N}_e$ from equations (38a)–(38b), we find that these equations are the same for A- and for S-combinations, so that without PF, the n_A and n_S would be identical and follow the blue dashed curve in figure 5(b). Preserving $\delta\hat{N}_e$ in equations (38a)–(38b) and plotting $n_{S,A}(P)$ (the black and red curves in figure 5(a)), we see that photon numbers $n_{S,A}$ are hardly affected by PF in the LED region, but PF lead to $n_S > n_A$ in the beginning of the intermediate region. From the end of the intermediate region and onwards, the PF suppress n_S making $n_S \ll n_A$ in the lasing region, where we also see that indeed $n_A \simeq n$, as we anticipated in section 5 to derive the central result equation (50) for the linewidth. Thus, due to PF above threshold, n_S is strongly suppressed and n_A increased by a factor of two.

Figures 6(a) and (b) shows the analogous results for a conventional (non-superradiant) laser, to be contrasted with the case of figures 5(a) and (b). The linewidth $\gamma_{las}(P)$ of the conventional laser departs more gradually from its asymptotics at low pump to the asymptotics for high pump. An even more conspicuous difference with superradiant lasers is that for the non-superradiant laser n_S never exceeds n_A. This is an indication that PF have a stronger effect on the superradiant lasers. But n_S and n_A are both clearly affected

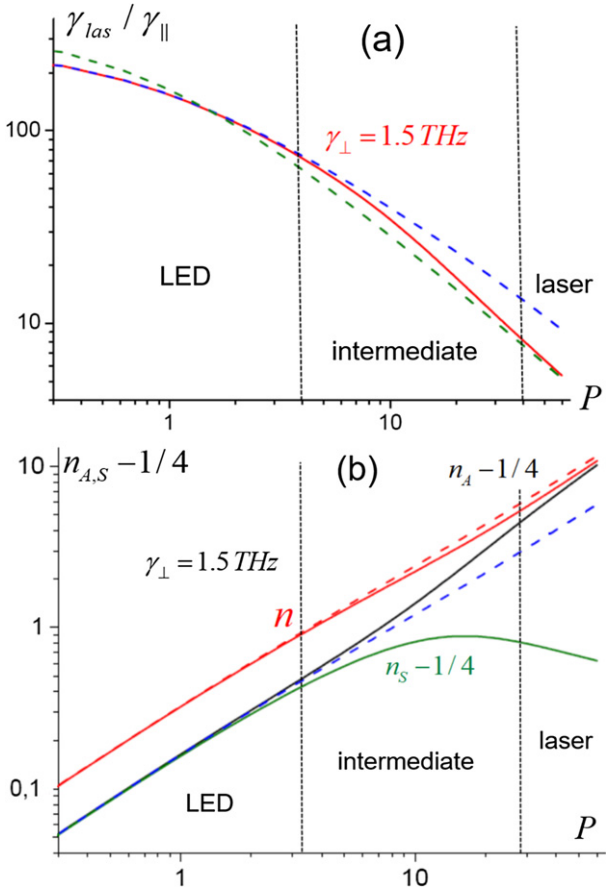

Figure 6. (a) Linewidth $\gamma_{las}(P)$ for non-superradiant laser with $\gamma_\perp^{max} = 1.5$ THz (red curve) and approximations for $\gamma_{las}(P)$ without population fluctuations (dashed blue curve) and for high pump (dashed olive curve). (b) Energies n_S of S- and n_A of A-fluctuations of the field of a non-superradiant laser. The blue dashed curve shows $n_A = n_S$ as found without population fluctuations. In contrast with the superradiant laser in figure 5(b), here $n_S < n_A$ everywhere. The same radiation regions as in figure 4(b) are separated by vertical dotted lines. The red solid line is the mean photon number n of equation (41), while the red dotted line is n without population fluctuations.

by PF for both types of lasers, and for both lasers $n_S \simeq 0$ and $n_A \simeq n$ at high pump rates. By contrast, both for the superradiant laser in figure 5(b) and for the conventional laser in figure 6(b), we see that the total number of photons practically does not depend on PF.

In the next section we will see that the larger PF of superradiant lasers will make their spectra qualitatively different from those of non-superradiant lasers.

6.2. Optical spectra

The different shapes of optical spectra for low and for high pump rates reflect different physical effects. It is therefore convenient to consider the spectra for high and for low pump rates separately.

Figure 7(a) shows optical spectra $n(\omega)$, given by equation (57), for a superradiant laser, with $2\kappa/\gamma_\perp^{min} = 2$, for high pump rates $P \geqslant 2$. Figure 7(b) shows the same for a non-superradiant laser, with $2\kappa/\gamma_\perp = 0.2$. Only in figure 7(a) for the superradiant laser do we see sideband peaks in the spectra.

These sideband peaks (or spikes) in $n(\omega)$ for curves 2 to 5 in figure 7(a) have the same nature as relaxation oscillations in lasers with $2\kappa \ll \gamma_\perp$ [36] that are described by rate equations. Sideband peaks appear because the carrier population reacts with some delay to changes in the field and polarization. The delay causes oscillatory energy exchange between the field, polarization and population with a resonance at the relaxation oscillation frequency. For $2\kappa \ll \gamma_\perp$, the relaxation oscillation frequency is given by ω_{ro}, as defined in equation (53) [36]. Such resonances cause well-known sidebands in the intensity fluctuation spectra [36, 41], see also figures 9(a) and (b) below. Analogous sideband peaks due to relaxation oscillations are not resolved in optical spectra of the non-superradiant laser with $2\kappa/\gamma_\perp = 0.2 \ll 1$ in figure 7(b). We attribute this to the fact that such a laser has smaller population fluctuations than a superradiant laser, as we have seen above in the analysis of the mean photon numbers, comparing figure 5(b) with figure 6(b).

For comparison, the dashed versions of curves 1, 2 and 3 show the corresponding spectra if population fluctuations are neglected. While curves 1 with and without population fluctuations are practically identical

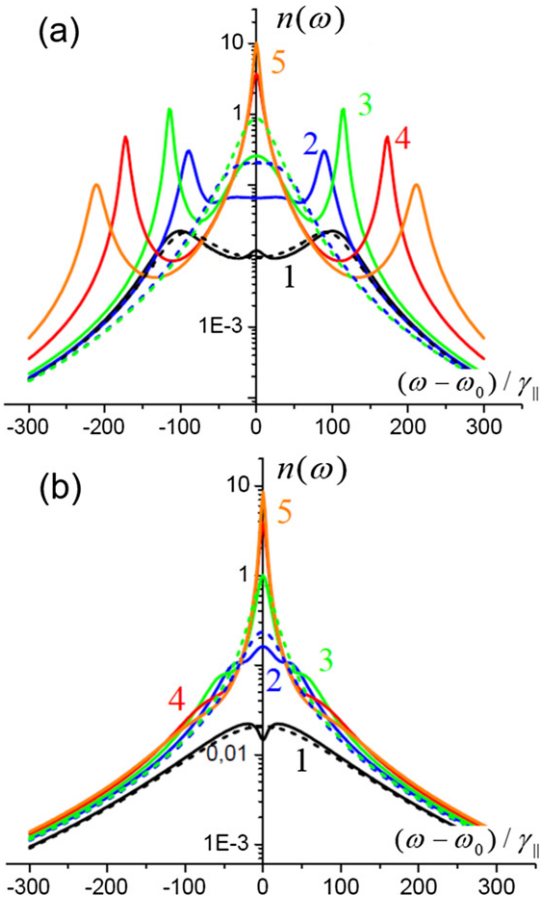

Figure 7. (a) Optical spectra of a superradiant laser with $\gamma_\perp^{\min} = 5 \times 10^{10}$ s^{-1} and $2\kappa/\gamma_\perp = 2$ and (b) of a non-superradiant laser with $\gamma_\perp = 5 \times 10^{11}$ s^{-1} and $2\kappa/\gamma_\perp = 0.2$, for pump rates $P = 2$ (curves 1); 8 (curves 2); 16 (curves 3); 28 (curves 4) and 40 (curves 5). The dashed curves are spectra found without population fluctuations, with the same parameters as for the solid curves 1, 2 and 3 of the same color.

(apart from a small structure in the center that we will discuss below), the dashed and solid curves 2 and 3 in figure 7(a) are qualitatively different: no sideband peaks are observed when population fluctuations are neglected. By contrast, solid and dashed curves are quite close to each other in figure 7(b) for the conventional (non-superradiant) laser, where population fluctuations are smaller than in the superradiant laser.

The two-peak structure in $n(\omega)$ for curve 1 in figure 7(a) has a different origin than the sideband peaks in curves 2–5 in this figure. The two broad peaks in curve 1 are due to CRS, which occurs when a large number of emitters exhibit Stark shifts in the lasing field. The parameters used for curve 1 satisfy the conditions for CRS, in particular $P < P_c$, see section 3 after equation (17). For curves 2 to 5, we have $P > P_c$, so CRS is absent. We described CRS in more detail in reference [59], but without taking population fluctuations into account.

Figures 8(a) and (b) show optical spectra for low pump rates $P \leqslant 2$. The two broad peaks in the curves in figure 8(a) are due to CRS. At these lower pump rates than previously considered in figure 7, population fluctuations lead to small features in the center of the optical spectra, namely a peak in figure 8(a) and a dip in figure 8(b). These small features arise due to nonlinearities. Mathematically, the denominator of equation (52) for $n_S(\omega)$ is a cubic polynomial of ω^2 and the spectrum $n(\omega)$ in equation (57) is a complicated function of ω^2.

Physically, the photons emitted at the frequencies of the two CRS peaks participate in a nonlinear scattering process: they induce population fluctuations, which couple to the polarization, and thereby have a back action on photon emission. In other words, photons may be re-absorbed and then emitted again by other emitters, which constitutes a nonlinear photon scattering process. Figure 8(a) shows that photons from both CRS peaks are re-absorbed and re-emitted most effectively near the center of the spectrum, leading to the small central peak in the optical spectra in figure 8(a).

Figure 8(b) shows the modification of the spectrum $n(\omega)$ due to the nonlinear photon scattering in a conventional (i.e. non-superradiant) laser, when conditions for CRS are not satisfied and CRS peaks are

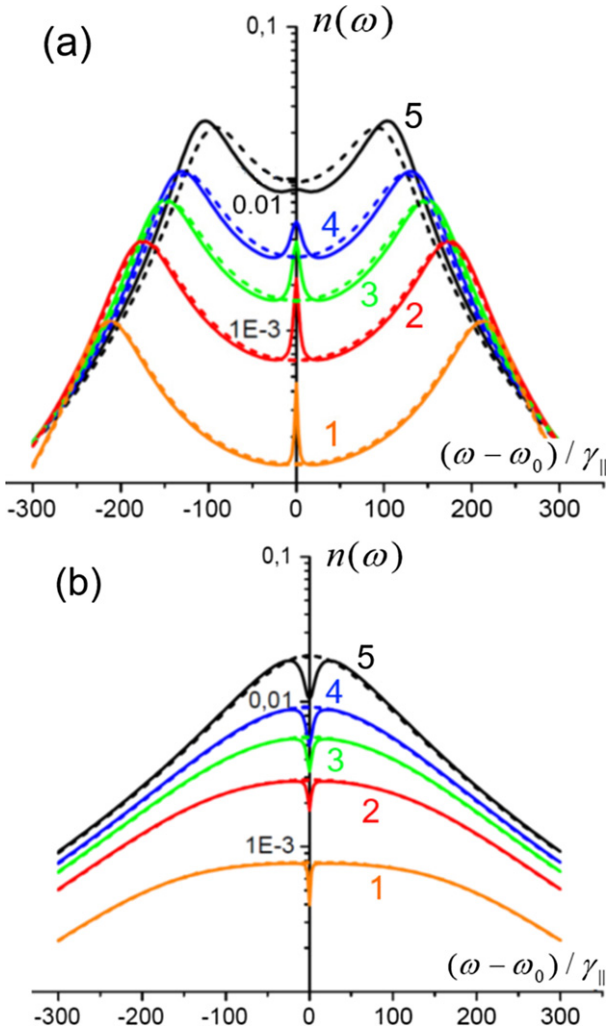

Figure 8. Spectra when weakly pumping (a) a superradiant laser with $\gamma_\perp^{\min} = 5 \times 10^{10}$ s^{-1} and $2\kappa/\gamma_\perp = 2$ and (b) a non-superradiant laser with $\gamma_\perp = 5 \times 10^{11}$ s^{-1} and $2\kappa/\gamma_\perp = 0.2$. The pump rates are $P = 0.16$ (curves 1); 0.48 (curves 2); 0.8 (curves 3); 1.12 (curves 4) and 2 (curves 5). Solid curves represent spectra with population fluctuations. For comparison, the corresponding dashed curves are found upon neglecting population fluctuations. Small structures (peaks and dips) in the centers of the spectra are due to nonlinear polarization induced by population fluctuations.

absent. Here, most emitters are near the center of the spectrum, and photons emitted in this spectral region are absorbed and re-emitted by all other emitters away from the center. By nonlinear scattering the energy of the field is thus taken from the center of the spectrum, where we see a dip, and re-emitted far from the center. Indeed we see that away from the dip, the solid curves in figure 8(b) lie slightly above the dashed curves, which do not take into account the nonlinear photon scattering.

For increasing pump rates, the main lasing peak grows, and the tiny nonlinear structures in the center of the lasing spectrum disappear.

From the solution of equation (38) it is difficult to say at what parameter values the peak in optical spectra at low excitations, as in figure 8(a), turns into a dip, as in figure 8(b). Calculations show that such a change depends on the competition of the first and the second terms in equation (38d). In particular, if we remove the first term in equation (38d), then at low excitation we will see only a small and narrow peak of width $\sim\gamma_\parallel$ in the optical spectra, a peak caused by the second term in equation (38d). In our theory the first term in equation (38d) at low excitation is obtained in a rough approximation. So, for the moment, we only have a qualitative prediction and physical interpretation of the small peaks or dips at low excitation in our model. We leave more quantitative investigations of these interesting structures for the future.

6.3. Spectra of intensity fluctuations

The radio-frequency spectrum of laser intensity fluctuations is important for applications of lasers in optical communications and can be measured by direct photodetection of the lasing field as fluctuations of the photocurrent [36]. Here we will derive an approximate expression for the intensity fluctuation spectra

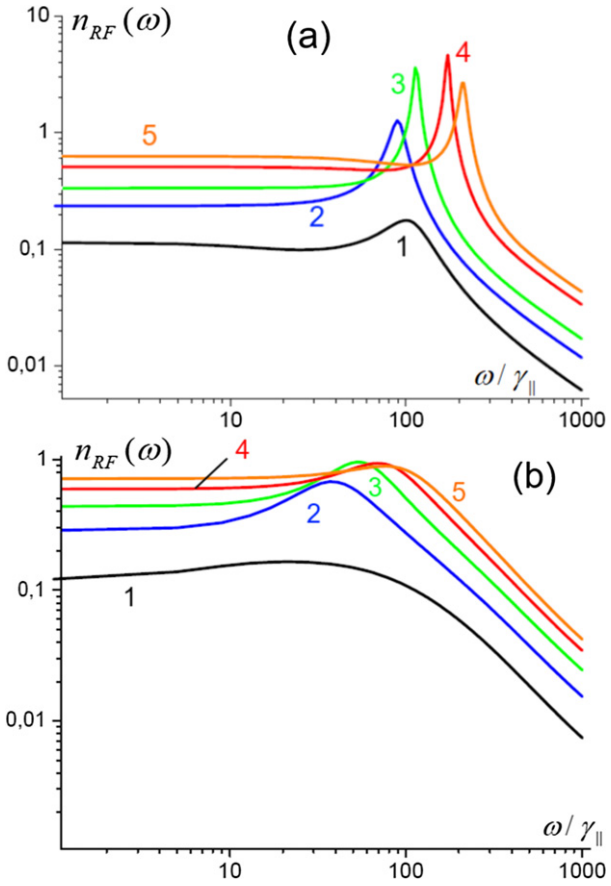

Figure 9. Photon number fluctuations in the high-pump limit for (a) a superradiant laser and (b) a non-superradiant laser. The parameters for the lasers and for the curves 1 to 5 are the same as in figures 7(a) and (b). Photon number fluctuations and relaxation oscillation peaks for the non-superradiant laser are much smaller than for the superradiant laser.

of our nanolasers, restricting ourselves to the high-pump limit, where almost all energy resides in the A-combinations of the quadratures.

Slow fluctuations of A-combinations, or equivalently phase fluctuations according to figure 3, can be neglected in calculations of photon number fluctuations. In this high-excitation limit, according to equations (28a) and (34),

$$\hat{a} \approx (\sqrt{n} + \hat{a}'_{\mathrm{S}})\mathrm{e}^{\mathrm{i}\pi/4}. \tag{59}$$

In equation (59) the operator $\hat{a}'_{\mathrm{S}}$ describes broadband amplitude fluctuations, and we take $\hat{a}'_{\mathrm{S}} = \hat{a}_{\mathrm{S}}$ where $\hat{a}_{\mathrm{S}}$ is found from equation (38). Then we obtain the photon number (or intensity) fluctuation spectrum

$$n_{\mathrm{RF}}(\omega) = 4nn_{\mathrm{S}}(\omega), \tag{60}$$

where $n_{\mathrm{S}}(\omega)$ is given by equation (52). In figure 9, photon number fluctuation spectra are shown for the same parameter values as in figure 7. In figures 9(a) and (b) one observes the well-known relaxation oscillation peaks [37, 69]. When $\gamma_{\perp}$ increases corresponding to the transition from a superradiant laser (figure 9(a)) to a conventional laser (figure 9(b)), the population fluctuations are reduced and the maxima of the relaxation oscillation peaks in $n_{\mathrm{RF}}(\omega)$ decrease. Similarly, the sideband peaks in the optical spectra of the superradiant laser shown in figure 7(a) disappear upon increasing $\gamma_{\perp}$, finally arriving to the case of the conventional laser with optical spectra as shown in figure 7(b). This similarity confirms that sideband peaks in optical spectra of a superradiant laser are caused by strong population fluctuations leading to strong relaxation oscillations.

7. Discussion

In this section we discuss our approach to linearize the MBE, followed by a discussion of the main results.

In the high-pump limit, equation (1) can be linearized around their mean values, when the field and polarization are sums of their coherent parts, which is a solution of the semiclassical equation (5), plus small fluctuations [36, 54, 55]. Such a linearization is equivalent to the SSA that is well-known in electrical

engineering [70] and which has also been applied to laser rate equations before [37, 71]. Rate equations can not be applied for superradiant lasers, where polarization is a dynamical variable.

The standard SSA of equation (1) cannot be applied in the low-pump limit, where the mean values of the lasing field and polarization vanish. In order to linearize the MBE in the low-pump limit, we made a first approximation within our new method in section 3 by neglecting population fluctuations with respect to the large mean-value population of the large number of emitters. This approximation gives satisfactory results when calculating mean values. An important example is the mean photon number, which is well described both below, near and above the semiclassical laser threshold. Also, the laser linewidth is accurately accounted for, at least below threshold. However, it is one of the main points of this paper that accounting for population fluctuations is necessary in order to correctly account for the linewidth of the laser above threshold, as well as the detailed structure of the laser spectrum below as well as above threshold.

We therefore made an improved analysis, where both the population fluctuations and the dynamics of the material polarization are taken into account. First we considered the high-pump limit in section 4, but again using an approach that differs from and extends the conventional SSA. The first difference is that we separate the mean values and fluctuations only in the *non*linear terms in the laser equation (1). A further difference is that we use the symmetric (S) and the anti-symmetric (A) combinations (34) of the quadratures. In figure 3 we showed that S-combinations are related to the amplitude and A-combinations to the phase of the lasing field. We arrived at two linear sets of equations: a set of two equations (38a) and (38b) for A-combinations and a set of three equations (38a), (38c) and (38d) for S-combinations of the quadratures coupled to population fluctuations. Our finding that population fluctuations are explicitly coupled to the S- but not to the A-combinations, is in agreement with the well-known fact [72] that variations in the carrier density change the gain, which subsequently changes the amplitude. If the alpha-parameter (linewidth enhancement factor) is zero, as in our case, the gain changes do not affect the phase.

Next we put forward the hypothesis that the linearized equation (38) as derived in the high-pump limit can be used in the intermediate- and in the low-pump limits as well, where they give satisfactory approximate predictions. First of all, if we neglect population fluctuations, then equation (38) become identical to the equation (10) that we derived for the low-pump limit in section 3.

Having discussed our new approach in detail, in the remaining part of this section we will discuss our new results.

We demonstrated that the well-known factor $1/2$ difference between the laser linewidth equation (23) for the low-pump limit and equation (50) for the high-pump limit arises due to population fluctuations. If we would neglect population fluctuations, then we would obtain the linewidth (23) for arbitrary pump rates. Furthermore, we calculated the laser linewidth at arbitrary pump rates, taking population fluctuations into account, and demonstrated a smooth transition between the limits for low and high pump rates, as shown in figures 5(a) and 6(a).

We calculated the full optical spectrum, given by equations (55) or (57). In the high-pump limit, the optical spectrum features a narrow peaked spectrum $n_{\mathrm{A}}(\omega)$, with a width determined by the phase fluctuations, on top of a broad background spectrum $n_{\mathrm{S}}(\omega)$, related to the amplitude fluctuations. Similar sharp 'coherent' peaks and 'incoherent' wings are seen in experiments, for example in figure 1 of reference [64] or, for superradiant lasers, in figure 4(b) of reference [20]. The usual analysis completely neglects this broad background emission in the optical spectra [35].

We found sidebands in the optical spectrum $n(\omega)$, shown in figure 7(a) for a superradiant laser with a high beta factor and a low-quality cavity ($2\kappa/\gamma_{\perp} \geqslant 1$). In this case, population fluctuations are especially important and the laser displays strong relaxation oscillations, which show up as sidebands in the optical spectra.

Another mechanism that gives rise to satellite peaks in optical spectra is well-known for semiconductor lasers. It arises because the refractive index depends on the level of excitation, as described by the so-called α-parameter in the rate equations [33]. However, this is not the mechanism leading to the sideband peaks in our model, where the frequency of the lasing field is exactly on resonance with the lasing transition and the α-parameter is zero.

For weak pumping, when the main lasing peak has not yet appeared, we predict small features in the center of the lasing spectra as displayed in figure 8. These small spectral peaks and dips only appear when taking population fluctuations into account. With our present theory we only make qualitative predictions about these small features, because we neglect the second-order correlations in equation (27c) although at low excitation these are of the same order of magnitude as the linear terms in this equation for population fluctuations $\delta\hat{N}_e$. From calculations that do account for these correlations, not shown in this paper, we find that the small central peaks and dips are preserved, but their heights and widths are changed. Below we give an interpretation why the central peak (dip) appears for the lasers parameters of figure 8(a) (figure 8(b)).

Population fluctuations (PF) at low excitation have a relatively high spectral power density in the range $\gamma_\parallel \ll \gamma_\perp, 2\kappa$ near zero frequency, where the PF are mostly due to the pump and the population decay noise. Far from the center of the spectrum on the other hand, the PF are caused by the interaction with the field and polarization, and the spectral density of PF is relatively small. Since $\gamma_\parallel$ is much smaller than the width of the spectra in figure 8, the PF can produce either a peak or a dip of width $\sim\gamma_\parallel$ in the center of the optical spectrum.

When CRS is absent, as in figure 8(b), then the maxima in the linear and nonlinear parts of the polarization coincide and interfere destructively in the frequency region of width $\gamma_\parallel$ around the center of the optical spectrum. The linear part of the polarization (i.e. the part that is independent of population fluctuations) induces the birth of a photon. This leads to a PF, which decreases the population of the upper level. Such a PF, in turn, leads to a polarization fluctuation, which suppress the birth of the next photon. This is a reason for a dip in the center of the optical spectra in figure 8(b).

The situation is different when the maxima of the linear part of the polarization are not in the center of the optical spectrum, as it happens when CRS occurs. Then the PF in the frequency region near the center of the spectrum are less affected by the lasing field, compared to the case without CRS. The field now resides mostly in CRS peaks far from the center, where the spectral power density of the PF is relatively small. The pump, therefore, increases the PF near the center of the spectrum, leading to a central peak, as shown in figure 8(a).

The new sideband peaks and fine structures of spectra of superradiant laser have not been seen in the experiments of references [20–22, 24, 25]. Based on our theory, we predict the kind of lasers and the parameter region, given after equation (58), in which to observe such features. The active medium should work in a three-level (effectively two-level) scheme. The sufficient conditions for a laser to be superradiant must be satisfied, i.e. $\tilde{\beta}_c \geqslant 1$ and $2\kappa \geqslant \gamma_\perp$. For example, one can reduce $\gamma_\perp$, so that $2\kappa \geqslant \gamma_\perp$, by lowering the temperature of a nanolaser with q-dots as the active medium [68]. Or vice versa, by increasing the temperature one can go from the superradiant to the non-superradiant regime in the same laser. The pump rate must be in the range from $\gamma_\parallel$ to $20\gamma_\parallel$, corresponding to the intermediate region (see figure 4(b)), where population fluctuations have their maximal effect, and the sideband peaks in optical spectrum (see figure 7(a)) can be observed. Lasers with possibly larger relaxation oscillation peaks in the intensity fluctuation spectrum, as in figure 9(a), are good candidates for observing sideband peaks in the optical spectrum as predicted here.

In our theory we have neglected inhomogeneous broadening of the active medium. This implies that for our current theory to be directly applicable, the actual inhomogeneous broadening must be much smaller than the distance between sideband peaks in the field spectra in figure 7(a). It was shown in reference [73] that collective effects synchronize emitters, even if the cavity linewidth is smaller than the inhomogeneous broadening. So we expect that some features in the spectra of SR lasers as discussed here will also show up in the presence of inhomogeneous broadening. More precise criteria for the observation of sideband peaks in the optical spectra of superradiant lasers will be derived from detailed investigations of the optical spectrum (57) in the future.

8. Conclusion

We presented a quantum theory for the spectra and fluctuations of a single-mode homogeneously broadened two-level laser. We developed a new approach, which does not employ the common approximation of eliminating the polarization adiabatically, meaning that the theory also applies to superradiant lasers with a low-quality cavity and a high beta factor. We linearised the equations, solved them and obtained analytical results.

We identify the LED region, where the laser linewidth described by equation (23) is wide as in references [57, 64], the lasing region with a narrow laser linewidth equation (50) in agreement with reference [67], and the intermediate region in between them.

Different from the rate-equation approaches of references [33–36], we describe a smooth transition between the linewidth equation (23) in the LED region and the linewidth equation (50) in the lasing region, as in figures 5(a) and 6(a). Furthermore, we calculated optical spectra, including phase and amplitude fluctuations, which respectively lead to a narrow peak and a wide background of the spectra at high excitation, as in figure 7.

For superradiant lasers in the intermediate region, we predict two sideband peaks in the optical spectra $n(\omega)$, as a consequence of strong relaxation oscillations induced by strong population fluctuations. The sideband structure in $n(\omega)$ disappears for a non-superradiant laser with smaller relaxation oscillations and weaker population fluctuations.

In the LED region, we predict a structure (peak or dip) in the center of the lasing spectrum that is caused by the interference of the linear and nonlinear parts of the polarisation. The interference is constructive, leading to a small peak in the center of the spectrum, if the linear part of polarisation displays CRS [59]. Otherwise the interference is destructive and then we predict a corresponding small dip in the center of the spectrum.

We expect that our approach and results will be useful also for further theoretical and experimental studies of spectra, fluctuations and correlations in superradiant lasers as, for example, in the nonstationary multimode superradiant lasers with hot normal modes [74], and in other lasers for a wide range of parameters, at any pump values and when the active-medium polarisation cannot be adiabatically eliminated.

In this paper we used our method only to calculate mean values and lasing spectra. In the future, our approach could also be used to calculate higher-order correlations, for example the second-order correlation function g_2 of the lasing field.

Acknowledgments

This work has been funded by Villum Fonden (VKR Center of Excellence NATEC-II, Grant 8692), and by the Danish National Research Foundation through NanoPhoton—Center for Nanophotonics (Grant No. DNRF147). MW acknowledges support from the Independent Research Fund Denmark—Natural Sciences (Project No. 0135-00403B). Igor Protsenko wishes to acknowledge the support of an Otto Moensted Visiting Professorship Grant (19-12-1159). Authors are grateful to referees for careful reading and positive estimation of our paper, in particularly for notes and questions of referee 2, which help us to improve the paper considerably.

Data availability statement

All data that support the findings of this study are included within the article (and any supplementary files).

Appendix A. Inter-emitter correlations

Here, we will estimate the contributions to SR lasing of collective effects, inter-emitter correlations, and collective spontaneous emission. We use the examples considered in the main text. By employing equations for mean values, we neglect the effect of population fluctuations, which have only a small influence on mean values. Such equations for mean values, for our model without adiabatic elimination of polarization, were derived in [62]. There inter-emitter correlations were introduced as

$$D = f^{-1}\sum_{i\neq j}\left\langle \hat{v}_i^{+}\hat{v}_j^{+}\right\rangle,$$

and $C(N) = D/(nN + N_e)$ as a measure of collective effects. C is the ratio of the rate of collective spontaneous emission into the lasing mode (proportional to D), and the combined rate of spontaneous and stimulated emission and absorption (proportional to $(nN + N_e)$). In the stationary case, the proportionality coefficient for all these rates is the lasing differential gain (i.e. gain per photon and per emitter). It was found in [62] that

$$C = \frac{(2\kappa/\gamma_\perp)N}{N_{\rm th} + (2\kappa/\gamma_\perp)(N_{\rm th} - N)}. \tag{A1}$$

We see that $C(N)$ is small at $2\kappa/\gamma_\perp \ll 1$; the minimum $C \sim -1$ at $N = -N_0$ and $2\kappa/\gamma_\perp \geqslant 1$; C increases with $2\kappa/\gamma_\perp$ and approaches $2\kappa/\gamma_\perp$ at large pump, when $N \to N_{\rm th}$. Thus, collective effects are important for low-Q cavities, in accordance with [17–19], when $2\kappa/\gamma_\perp \geqslant 1$.

Figure 10 shows $C(P)$ for two examples, used above, with $\gamma_\perp = 50$ GHz, $2\kappa/\gamma_\perp = 2$ and with $\gamma_\perp = 500$ GHz, $2\kappa/\gamma_\perp = 0.2$. We see that for the laser with the low-Q cavity and $2\kappa/\gamma_\perp = 2$, the variable C varies much more as a function of pump rate than for the laser with a high-Q cavity characterized by $2\kappa/\gamma_\perp = 0.2$. For high pump $C > 1$ at $2\kappa/\gamma_\perp = 2$, so the collective spontaneous-emission rate exceeds the rates of stimulated and spontaneous emission and of absorption. At low pump in a low-Q cavity laser, the inter-emitter correlations lead to strong excitation trapping, so that spontaneous emission into the lasing mode is suppressed almost completely: $D \approx -(nN + N_e)$ so that $C \to -1$, although C does not reach -1 exactly.

The stationary radiation rate $R_{\rm rad}$ into the lasing mode found in [62] is

$$R_{\rm rad} = \gamma_{\parallel}\tilde{\beta}_c[Nn + N_e + (2\kappa/\gamma_\perp)Nn]. \tag{A2}$$

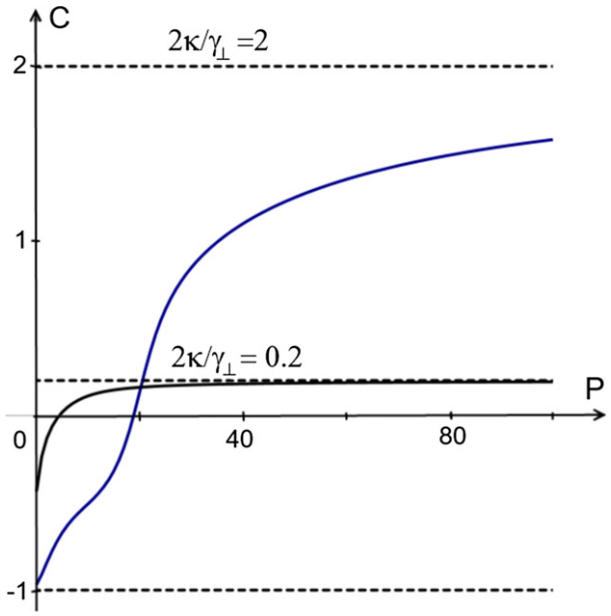

Figure 10. Parameter C, characterising collective effects, as a function of pump for a superradiant laser with $2\kappa/\gamma_\perp = 2$ (blue curve) and for a non-superradiant laser with $2\kappa/\gamma_\perp = 0.2$ (black curve). Horizontal dashed lines show maximum values of $C(P)$ for SR and non-SR lasing, and the minimum $C(P) = -1$, when spontaneous emission into the lasing mode is fully suppressed due to excitation trapping.

Here the first term Nn describes stimulated emission and absorption, the second term N_e describes spontaneous emission into the lasing mode, while the last term $(2\kappa/\gamma_\perp)Nn = D$ is responsible for collective spontaneous emission into the lasing mode. One can introduce a beta-factor $\tilde{\beta}_{\rm SR} = R_{\rm rad}/\gamma_\parallel N_e$, where $\gamma_\parallel N_e$ is the rate of all losses of the upper-level population, except the radiative one. $\tilde{\beta}_{\rm SR}$ takes into account collective emission into the lasing mode

$$\tilde{\beta}_{\rm SR} = \tilde{\beta}_c[1 + (2\kappa/\gamma_\perp)nN/N_e]. \tag{A3}$$

For $N < 0$ we have $\tilde{\beta}_{\rm SR} < \tilde{\beta}_c$, which implies subradiance due to population trapping. For $N > 0$ we have $\tilde{\beta}_{\rm SR} > \tilde{\beta}_c$, so that SR increases the radiation rate into the lasing mode and helps to reach lasing.

We see in figure 4(b) that the population inversion N approaches $N_{\rm th}$ in the lasing region. So in order to reach lasing, the number of emitters N_0 must be large: $N_0 > N_{\rm th}$. This condition may be written as $\tilde{\beta} > 2\kappa/(N_0\gamma_\parallel)$ or, with our values of parameters, $\tilde{\beta} > 1/2$. Taking $\beta = \tilde{\beta}/(1+\tilde{\beta})$ we obtain that in our case $\beta > 1/3$ both for SR lasing at $2\kappa/\gamma_\perp > 1$ and for non-SR lasing at $2\kappa/\gamma_\perp \ll 1$. We conclude that in our case the SR lasing conditions are $2\kappa/\gamma_\perp \geqslant 1$ and $\beta \geqslant 1$.

Appendix B. Diffusion coefficients

The Heisenberg–Langevin equation for an operator $\hat{Q}_\alpha$ is

$$\mathrm{d}\hat{Q}_\alpha/\mathrm{d}t = \hat{M}_\alpha + \hat{F}_\alpha, \tag{B1}$$

where $\hat{F}_\alpha$ is the Langevin force, with properties

$$\langle \hat{F}_\alpha \rangle = 0, \langle \hat{F}_\alpha(t)\hat{F}_\beta(t')\rangle = 2D_{\alpha\beta}\delta(t-t').$$

Here the diffusion coefficient $2D_{\alpha\beta}$ is determined from the 'generalized Einstein formula'

$$2D_{\alpha\beta} = \mathrm{d}\langle \hat{Q}_\alpha\hat{Q}_\beta\rangle/\mathrm{d}t - \langle \hat{M}_\alpha\hat{Q}_\beta\rangle - \langle \hat{Q}_\alpha\hat{M}_\beta\rangle. \tag{B2}$$

If we denote the upper (lower) state of the ith emitter by $|e\rangle_i$ ($|g\rangle_i$), then $\hat{\sigma}_i = |g\rangle_i\langle e|_i$, $\hat{\sigma}_i^+ = |e\rangle_i\langle g|_i$ and $\hat{n}_i^{(\alpha)} = |\alpha\rangle_i\langle\alpha|_i$, for $\alpha = \{e, g\}$. Using the orthogonality of the states $\langle\alpha|_i|\beta\rangle_j = \delta_{\alpha\beta}\delta_{ij}$, we obtain $\hat{\sigma}_i^+\hat{\sigma}_j = \hat{n}_i^{(e)}\delta_{ij}$ and therefore $\hat{v}^+\hat{v} = f\hat{N}_e$, where $\hat{v}$ and f are the same as in equation (1).

From equation (B2) we find

$$2D_{v^+v} = f[\gamma_\perp N_e + \gamma_\parallel (PN_g - N_e)]. \tag{B3}$$

The second term $\sim\gamma_\parallel$ in equation (B3) is due to population fluctuations. Population fluctuations are small and, in general, change mean values only slightly, as illustrated for example for $n(P)$ in figures 5(b) and 6(b). The same is true for equation (B3), where the second term can be neglected for not too high pumping, when $\gamma_\perp \geqslant \gamma_\parallel P$. In calculations we see that the second term in equation (B3) has only a small influence on the results. So for our examples with $\gamma_\perp \leqslant \gamma_\parallel P$, we take $2D_{v^+v} \approx f\gamma_\perp N_e$.

There is one more reason for the approximation $2D_{v^+v} \approx f\gamma_\perp N_e$. Taking $\hat{a}(\omega)$ given by equation (12), the diffusion coefficient (B3) and $2D_{a^+a} = 0$, we find the commutator

$$\langle[\hat{a}, \hat{a}^+]\rangle = 1 - \frac{4\kappa n}{\gamma_\perp (N_{\rm th} + N_0)} \left(2n + \frac{1}{1 + 2\kappa/\gamma_\perp}\right).$$

The mismatch with $\langle[\hat{a}, \hat{a}^+]\rangle = 1$ comes from the second term on the right in equation (B3). This example shows that usage of exact diffusion coefficients in combination with approximate equations is an excess of accuracy and may lead to the breaking of commutation relations.

If $\hat{Q}_{\gamma_i} = \hat{Q}_{\alpha_i} + \hat{Q}_{\beta_i}$ then

$$2D_{\gamma_1\gamma_2} = 2D_{\alpha_1\alpha_2} + 2D_{\beta_1\alpha_2} + 2D_{\beta_2\alpha_1} + 2D_{\beta_1\beta_2}, \tag{B4}$$

as it follows from equation (B2). From equation (B2) we find

$$2D_{vv^+} = f[\gamma_\perp N_g - \gamma_\parallel (PN_g - N_e)], 2D_{aa^+} = 2\kappa, \tag{B5}$$

while the remaining diffusion coefficients for $\hat{a}$, $\hat{a}^+$, $\hat{v}$, $\hat{v}^+$ all vanish. From equations (B3)–(B5) we obtain the diffusion coefficients (46) of the main text.

Using the operator relations $\hat{N}_e\hat{N}_e = \hat{N}_e$ and $\hat{N}_e\hat{N}_g = 0$, we obtain $2D_{N_eN_e}$ in equation (54) of the main text.

Appendix C. Stationary solutions

In this appendix we derive expressions for the stationary population inversion and photon number both below and above threshold.

First we consider the situation below threshold. We solve equation (21) and find the stationary population inversion

$$N(P) = \frac{N_{\rm th}}{2(P+1)} \left[2(P-1)N_0/N_{\rm th} - M_b - \sqrt{Q_b}\right], \tag{C1a}$$

where $M_b = (P-1)N_0/N_{\rm th} - P - 1 - \tilde{\beta}_c$ and $Q_b = M_b^2 + 8P\tilde{\beta}_c N_0/N_{\rm th}$. After that we determine the stationary photon number $n(P)$ from the energy conservation law equation (4) and find

$$n(P) = \frac{1}{4\tilde{\beta}} \left(M_b + \sqrt{Q_b}\right). \tag{C1b}$$

Next we do the analogous analysis in the high-excitation limit. In this case, almost all photons are in the A-combination of quadratures, so in equation (49) we set $n_{\rm A} = n$ and we neglect the constant term $2\kappa/\gamma_\perp$ with respect to the term $\sim 1/(N_{\rm th} - N)$ that gets large when $N \to N_{\rm th}$ at high pump. By inserting this photon number n into equation (4) we again arrive at a quadratic equation for N,

$$\tilde{\beta}_c(N_0 + N_{\rm th})/2 = [P(N_0 - N) - N_0 - N](1 - N/N_{\rm th}).$$

Solving this equation and using the energy conservation law equation (4), we find solutions N and n that are again given by equation (C1a), but now with the coefficients

$$M_a = (P-1)N_0/N_{\rm th} - P - 1,$$

$$Q_a = M_a^2 + 2(P+1)\tilde{\beta}_c(N_0/N_{\rm th} + 1),$$

instead of M_b and Q_b, respectively.

ORCID iDs

Martijn Wubs https://orcid.org/0000-0002-8286-7825

References

[1] Noda S, Kitamura K, Okino T, Yasuda D and Tanaka Y 2017 Photonic-crystal surface-emitting lasers: review and introduction of modulated-photonic crystals *IEEE J. Sel. Top. Quantum Electron.* **23** 1
[2] Noda S 2006 Seeking the ultimate nanolaser *Science* **314** 260
[3] Prieto I *et al* 2015 Near thresholdless laser operation at room temperature *Optica* **2** 66
[4] Takiguchi M *et al* 2016 Systematic study of thresholdless oscillation in high-β buried multiple-quantum-well photonic crystal nanocavity lasers *Opt. Express* **24** 3441
[5] Ota Y, Kakuda M, Watanabe K, Iwamoto S and Arakawa Y 2017 Thresholdless quantum dot nanolaser *Opt. Express* **25** 19981
[6] Nozaki K, Kita S and Baba T 2007 Room temperature continuous wave operation and controlled spontaneous emission in ultrasmall photonic crystal nanolaser *Opt. Express* **15** 7506
[7] Yu Y, Xue W, Semenova E, Yvind K and Mork J 2017 Demonstration of a self-pulsing photonic crystal fano laser *Nat. Photon.* **11** 81
[8] Li Y, Wang L, Li L and Tong L 2019 Optical microfiber-based ultrafast fiber lasers *Appl. Phys.* B **125** 192
[9] Lermer M *et al* 2013 High beta lasing in micropillar cavities with adiabatic layer design *Appl. Phys. Lett.* **102** 052114
[10] Kreinberg S, Chow W W, Wolters J, Schneider C, Gies C, Jahnke F, Höfling S, Kamp M and Reitzenstein S 2017 Emission from quantum-dot high-β microcavities: transition from spontaneous emission to lasing and the effects of superradiant emitter coupling *Light: Sci. Appl.* **6** e17030
[11] Suh J Y, Kim C H, Zhou W, Huntington M D, Co D T, Wasielewski M R and Odom T W 2012 Plasmonic Bowtie nanolaser arrays *Nano Lett.* **12** 5769
[12] Khajavikhan M, Simic A, Katz M, Lee J H, Slutsky B, Mizrahi A, Lomakin V and Fainman Y 2012 Thresholdless nanoscale coaxial lasers *Nature* **482** 204
[13] Kurosaka Y, Iwahashi S, Liang Y, Sakai K, Miyai E, Kunishi W, Ohnishi D and Noda S 2010 On-chip beam-steering photonic-crystal lasers *Nat. Photon.* **4** 447
[14] Zhou W, Liu S-C, Ge X, Zhao D, Yang H, Reuterskiöld-Hedlund C and Hammar M 2019 On-chip photonic crystal surface-emitting membrane lasers *IEEE J. Sel. Top. Quantum Electron.* **25** 1
[15] Crosnier G, Sanchez D, Bouchoule S, Monnier P, Beaudoin G, Sagnes I, Raj R and Raineri F 2017 Hybrid indium phosphide-on-silicon nanolaser diode *Nat. Photon.* **11** 297
[16] Purcell E M 1946 Spontaneous emission probabilities at radio frequencies *Phys. Rev.* **69** 681
[17] Khanin Y I 1995 *Principles of Laser Dynamics* (Amsterdam: North-Holland)
[18] Belyanin A A, Kocharovsky V V and Kocharovsky V V 1998 Superradiant generation of femtosecond pulses in quantum-well heterostructures *Quantum Semiclass. Opt.* **10** L13
[19] Temnov V V 2005 Superradiance and subradiance in the overdamped many-atom micromaser *Phys. Rev.* A **71** 053818
[20] Norcia M A and Thompson J K 2016 Cold-strontium laser in the superradiant crossover regime *Phys. Rev.* X **6** 011025
[21] Schäffer S A, Christensen B T R, Henriksen M R and Thomsen J W 2017 Dynamics of bad-cavity-enhanced interaction with cold Sr atoms for laser stabilization *Phys. Rev.* A **96** 013847
[22] Meiser D and Holland M J 2010 Steady-state superradiance with alkaline-earth-metal atoms *Phys. Rev.* A **81** 033847
[23] Debnath K, Zhang Y and Mølmer K 2018 Lasing in the superradiant crossover regime *Phys. Rev.* A **98** 063837
[24] Bohnet J G, Chen Z, Weiner J M, Meiser D, Holland M J and Thompson J K 2012 A steady-state superradiant laser with less than one intracavity photon *Nature* **484** 78
[25] Jahnke F *et al* 2016 Giant photon bunching, superradiant pulse emission and excitation trapping in quantum-dot nanolasers *Nat. Commun.* **7** 11540
[26] Bhatti D, von Zanthier J and Agarwal G S 2015 Superbunching and nonclassicality as new hallmarks of superradiance *Sci. Rep.* **5** 17335
[27] Zhou Y, Li F-l, Bai B, Chen H, Liu J, Xu Z and Zheng H 2017 Superbunching pseudothermal light *Phys. Rev.* A **95** 053809
[28] Schawlow A L and Townes C H 1958 Infrared and optical masers *Phys. Rev.* **112** 1940
[29] Haken H 1964 Theory of coherence of laser light *Phys. Rev. Lett.* **13** 329
[30] Scully M O and Lamb W E 1967 Quantum theory of an optical maser. I. General theory *Phys. Rev.* **159** 208
[31] Haken H 1984 *Laser Theory* (Berlin: Springer)
[32] Kelley P L, Lax B and Tannenwald P E 1966 *Physics of Quantum Electronics* (New York: McGraw-Hill)
[33] Henry C 1986 Phase noise in semiconductor lasers *J. Lightwave Technol.* **4** 298
[34] Henry C 1983 Theory of the phase noise and power spectrum of a single mode injection laser *IEEE J. Quantum Electron.* **19** 1391
[35] Vahala K and Yariv A 1983 Semiclassical theory of noise in semiconductor lasers—part I *IEEE J. Quantum Electron.* **19** 1096
[36] Yamamoto Y 1983 AM and FM quantum noise in semiconductor lasers—part I: theoretical analysis *IEEE J. Quantum Electron.* **19** 34
[37] McKinstrie C J 2020 Stochastic and probabilistic equations for three- and four-level lasers: tutorial *J. Opt. Soc. Am.* B **37** 1333
[38] Mork J and Lippi G L 2018 Rate equation description of quantum noise in nanolasers with few emitters *Appl. Phys. Lett.* **112** 141103
[39] Auffèves A, Gerace D, Portolan S, Drezet A and França Santos M 2011 Few emitters in a cavity: from cooperative emission to individualization *New J. Phys.* **13** 093020
[40] Mascarenhas E, Gerace D, Santos M F and Auffèves A 2013 Cooperativity of a few quantum emitters in a single-mode cavity *Phys. Rev.* A **88** 063825
[41] Moelbjerg A, Kaer P, Lorke M, Tromborg B and Mork J 2013 Dynamical properties of nanolasers based on few discrete emitters *IEEE J. Quantum Electron.* **49** 945
[42] Gies C, Wiersig J, Lorke M and Jahnke F 2007 Semiconductor model for quantum-dot-based microcavity lasers *Phys. Rev.* A **75** 013803
[43] Meiser D, Ye J, Carlson D R and Holland M J 2009 Prospects for a millihertz-linewidth laser *Phys. Rev. Lett.* **102** 163601
[44] Kirton P and Keeling J 2018 Superradiant and lasing states in driven-dissipative Dicke models *New J. Phys.* **20** 015009
[45] Jäger S B, Holland M J and Morigi G 2020 Superradiant optomechanical phases of cold atomic gases in optical resonators *Phys. Rev.* A **101** 023616
[46] Zhang Y, Zhang Y-X and Mølmer K 2018 Monte-Carlo simulations of superradiant lasing *New J. Phys.* **20** 112001

[47] Vasil'ev P P and Penty R V 2020 Wigner function and photon number distribution of a superradiant state in semiconductor heterostructures *New J. Phys.* **22** 083046
[48] Ostermann L, Meignant C, Genes C and Ritsch H 2019 Super- and subradiance of clock atoms in multimode optical waveguides *New J. Phys.* **21** 025004
[49] Suarez E, Auwärter D, Arruda T J, Bachelard R, Courteille P W, Zimmermann C and Slama S 2019 Photon-antibunching in the fluorescence of statistical ensembles of emitters at an optical nanofiber-tip *New J. Phys.* **21** 035009
[50] Scully M S and Zubairy M O 1997 *Quantum Optics* (Cambridge: Cambridge University Press)
[51] Duan L-M, Giedke G, Cirac J I and Zoller P 2000 Inseparability criterion for continuous variable systems *Phys. Rev. Lett.* **84** 2722
[52] Feyisa C G 2020 Enhanced CV entanglement quantification in a CEL with parametric amplifier and coupled to squeezed vacuum *Braz. J. Phys.* **50** 379
[53] Pegg D T and Barnett S M 1989 Phase properties of the quantized single-mode electromagnetic field *Phys. Rev.* A **39** 1665
[54] Davidovich L 1996 Sub-Poissonian processes in quantum optics *Rev. Mod. Phys.* **68** 127
[55] Kolobov M I, Davidovich L, Giacobino E and Fabre C 1993 Role of pumping statistics and dynamics of atomic polarization in quantum fluctuations of laser sources *Phys. Rev.* A **47** 1431
[56] Butylkin V, Khronopulo Y, Kaplan A E and Yakubovich E I 1989 *Resonant Nonlinear Interactions of Light with Matter* (Berlin: Springer)
[57] Yariv A 1967 *Quantum Electronics* (New York: Wiley)
[58] Protsenko I, Domokos P, Lefèvre-Seguin V, Hare J, Raimond J M and Davidovich L 1999 Quantum theory of a thresholdless laser *Phys. Rev.* A **59** 1667
[59] André E C, Protsenko I E, Uskov A V, Mørk J and Wubs M 2019 On collective Rabi splitting in nanolasers and nano-LEDs *Opt. Lett.* **44** 1415
[60] Rice P R and Carmichael H J 1994 Photon statistics of a cavity-QED laser: a comment on the laser-phase-transition analogy *Phys. Rev.* A **50** 4318
[61] Siegman A E 1986 *Lasers* (Mill Valley, CA: University Science Books)
[62] Protsenko I E, André E, Uskov A V, Mørk J and Wubs M 2017 Collective effects in nanolasers explained by generalized rate equations (arXiv:1709.08200)
[63] Sargent M, Scully M O and Lamb W E 1974 *Laser Physics* (Reading, MA: Addison-Wesley Developers Press)
[64] Kuppens S J M, van Exter M P and Woerdman J P 1994 Quantum-limited linewidth of a bad-cavity laser *Phys. Rev. Lett.* **72** 3815
[65] Pollnau M and Eichhorn M 2020 Spectral coherence, part I: passive-resonator linewidth, fundamental laser linewidth, and Schawlow–Townes approximation *Prog. Quantum Electron.* **72** 100255
[66] Oraevsky A N 1988 Quantum fluctuations and formation of coherency in lasers *J. Opt. Soc. Am.* B **5** 933
[67] van Exter M P, Kuppens S J M and Woerdman J P 1995 Theory for the linewidth of a bad-cavity laser *Phys. Rev.* A **51** 809
[68] Bockelmann U and Egeler T 1992 Electron relaxation in quantum dots by means of Auger processes *Phys. Rev.* B **46** 15574
[69] Yamamoto Y, Saito S and Mukai T 1983 AM and FM quantum noise in semiconductor lasers—part II: comparison of theoretical and experimental results for AlGaAs lasers *IEEE J. Quantum Electron.* **19** 47
[70] Attenborough M 2003 *Mathematics for Electrical Engineering…* (Amsterdam: Newnes)
[71] Zali A R, Moravvej-Farshi M K, Yu Y and Mork J 2018 Small and large signal analysis of photonic crystal fano laser *J. Lightwave Technol.* **36** 5611
[72] Coldren L A, Corzine S W and Masanovic M L 2012 *Diode Lasers and Photonic Integrated Circuits* 2nd edn (New York: Wiley)
[73] Debnath K, Zhang Y and Mølmer K 2019 Collective dynamics of inhomogeneously broadened emitters coupled to an optical cavity with narrow linewidth *Phys. Rev.* A **100** 053821
[74] Kocharovsky V V, Zheleznyakov V V, Kocharovskaya E R and Kocharovsky V V 2017 Superradiance: the principles of generation and implementation in lasers *Phys.-Usp.* **60** 345